



Potential encoding of coupling between Milankovitch forcing and Earth's interior processes in the Phanerozoic eustatic sea-level record

Slah Boulila^{a,b,*}, Bilal U. Haq^{a,c}, Nathan Hara^d, R. Dietmar Müller^e, Bruno Galbrun^a, Guillaume Charbonnier^a

^a Sorbonne Université, CNRS, Institut des Sciences de la Terre Paris, IStEP, F-75005 Paris, France

^b ASD/IMCCE, CNRS-UMR8028, Observatoire de Paris, PSL University, Sorbonne Université, 77 Avenue Denfert-Rochereau, 75014 Paris, France

^c Smithsonian Institution, Washington, DC, USA

^d Département d'astronomie, Université de Genève, 51 Chemin de Pegasi b, 1290 Versoix, Switzerland

^e EarthByte Group, School of Geosciences, University of Sydney, Sydney, New South Wales 2006, Australia

ARTICLE INFO

Keywords:

Earth's climate

Sea level

Milankovitch

Tectonics

Multi-million year timescales

ABSTRACT

The driving mechanisms of Earth's climate system at a multi-Myr timescale have received considerable attention since the 1980's as they are deemed to control large-amplitude climatic variations that result in severe biogeochemical disruptions, major sea-level variations, and the evolution of Earth's land- and seascapes through geological time. The commonly accepted mechanism for these changes derives from the evolution of Earth's coupled plate-mantle system. Connection between Earth's interior and external climate drivers, e.g., Milankovitch insolation forcing, has not been investigated at multi-Myr timescale, because tectonics and astronomical influences at these longer timescales have long been thought as independent pacemakers in the evolution of the Earth system.

Here we have analyzed time-series from multiple geological datasets and found common periodicities of 10 and 35 Myr. Additionally, we have highlighted the modulation in amplitude of the 10 Myr cycle band by the 35 Myr cyclicity in sedimentary sea-level data. We then demonstrate the same physical amplitude modulation relationship between these two cyclicities in astronomical (Milankovitch) variations, and establish correlation between Milankovitch and sea-level variations at these two frequency bands. The 10 and 35 Myr cycles are prominent in the geological records, suggesting either unresolved fundamental Milankovitch periodicities, or reflecting a sedimentary energy-transfer process from higher to lower Milankovitch frequencies, as argued here via amplitude modulation analysis in both astronomical and sea-level data.

Finally, we find a coherent correlation, at the 35 Myr cycle band, between Milankovitch, sea-level and geodynamic (plate subduction rate) variations, hinting at a coupling between Earth's interior and surface processes via Milankovitch paced climate. Thus, our findings point to a coupling between Milankovitch and Earth's internal forcings, at 10 to 10s of Myr. The most likely scenario that could link insolation-driven climate change to Earth's interior processes is Earth's interior feedbacks to astro-climatically driven mass changes on Earth's surface. We suggest that Earth's interior processes may drive large-amplitude sea-level changes, especially during greenhouse periods, by resonating to astro-climatically driven Earth's surface perturbations.

1. Introduction

The link between Earth's interior and surface processes at longer geological timescales has fascinated Earth science community because their combined effect shapes the Earth's surface (e.g., Raymo et al., 1988; Molnar and England, 1990; Raymo and Ruddiman, 1992; Lamb and Davis, 2003; Lagabrielle et al., 2009; Whipple, 2009; Cloetingh and

Haq, 2015).

That solid Earth responds to or resonates with the Earth's surface perturbations induced by climate and environmental changes has been suggested at short timescales on the diurnal to annual band. Tidal forcing of the micro-seismic and volcanic activity has been argued based on several datasets (Johnston and Mauk, 1972; McNutt and Beavan, 1981; Emter, 1997; Petrosino et al., 2018; Dinger et al., 2019, among

* Corresponding author at: Sorbonne Université, CNRS, Institut des Sciences de la Terre Paris, IStEP, F-75005 Paris, France.

E-mail address: slah.boulila@sorbonne-universite.fr (S. Boulila).

many others). Also, correlations are well established between volcanic eruptions and diurnal to annual temperature and atmospheric pressure, suggesting that the hydrological cycle plays a crucial role in volcanism via water-mass transfer from oceans to continents and the resulting pressure changes on the upper mantle (see e.g., McNutt and Beavan, 1980; Neuberg, 2000; Mason et al., 2004).

Processes reflecting Earth's interior dynamics have been linked to climate change at millennial timescale (Rampino et al., 1979; McGuire et al., 1997; Huybers and Langmuir, 2009, 2017; Lund and Asimow, 2011; Kutterolf et al., 2012; Crowley et al., 2015; Tolstoy, 2015; Schindlbeck et al., 2018; Cerpa et al., 2019). In particular, the detection of shorter Milankovitch climate periodicities in global volcanic activity (Rampino et al., 1979; Schindlbeck et al., 2018) and in the seafloor abyssal bathymetry suggest links between astro-climate and Earth's interior processes (Crowley et al., 2015; Tolstoy, 2015). Such potential connections have been investigated by others, e.g., Olive et al. (2015) and Goff et al. (2018), who have suggested that Milankovitch forcing of sea-level (and thus seafloor abyssal hills) should not be taken at face value, and that only slow-spreading rates would favor such expression of Milankovitch periodicities in the bathymetric data. For fast- to intermediate-spreading rates, Olive et al. (2015) favor a tectono-magmatic model for the abyssal hill fabrics that considers normal faulting as an important element. This model differs from that based only on the magmatic and volcanic outputs at mid-ocean ridges to explain the fabric of the abyssal hills (Crowley et al., 2015; Tolstoy, 2015). Interestingly, Olive et al. (2015) suggested that the lithosphere and seafloor-shaping processes may act as a lowpass filter on variations in magma supply, damping Milankovitch periods shorter than about 100 kyr.

Another line of evidence for the potential connection between Earth's interior processes and external climate forcing, but at multi-Myr timescales, comes from a striking correlation between orbitally paced 9.5 Myr climatic cyclicity (from deep-sea stable oxygen-isotopic records, e.g., Zachos et al., 2001), and geodynamically-induced (tectonics, volcanism) oceanic-climatic events of the past 115 Ma (Boulila, 2019).

Major tectonic plate motions that occur at very slow, Myr to multi-Myr timescales, drive the evolution of land- and seascapes (Cloetingh and Haq, 2015), dictate changes in biomass evolution and turnovers, and drive biogeochemical and sea-level cycles. One of the major manifestations of long-term tectonic forcing is global sea-level eustatic variations through geodynamically-induced changes in the volume of the ocean basins (Vail et al., 1977; Haq et al., 1987; Miller et al., 2005a; Müller et al., 2008; Simmons, 2012; Conrad, 2013; Simmons et al., 2020). The recognition of similar periodicities in sea-level, climate and Milankovitch variations has led some researchers to suggest potential correlation between Milankovitch and tectonic forcings at multi-Myr timescales (Boulila, 2019; Boulila et al., 2020). Thus, the detection of correlatable Myr to multi-Myr scale variations in tectonic, biogeochemical, climate and sea-level proxy data (Vail et al., 1977; Haq et al., 1987; Boulila et al., 2011, 2012, 2018, 2020; Boulila, 2019) could provide further constraints for the link between Earth's interior and surface processes.

Here we review cyclicities of tens of Myr in astronomical and geological data. We focus on sedimentary inferred sea-level record and geodynamic data/models, and compare them with stable oxygen isotopes and astronomical (Milankovitch) variations. Given that Milankovitch variations exhibit modulation in amplitude and frequency, we performed amplitude modulation analysis (see Section 2.3) on Earth's orbital eccentricity variations to investigate the record of longer cyclicities of tens of Myr. Then, we performed amplitude modulation analysis on Phanerozoic sea-level data. Finally, we compared sea-level, climate and Milankovitch variations with geodynamic data for potential linkages.

2. Data and methods

2.1. Geological data

The eustatic sea level curve for the Phanerozoic was constructed based on sequence-stratigraphic studies of the marine sedimentary sections around the world. Correlations are based on the available marine biostratigraphic markers, and if a sea-level change can be demonstrated to be present in a number of non-contiguous sections, it is considered wide-spread and therefore eustatic. The details of these methodologies are described in Haq et al. (1987) for the Meso-Cenozoic and in Haq and Schutter (2008) for the Paleozoic. The Ceno-Mesozoic eustatic curve (Haq et al., 1987) was revised through a comparison with the Arabian Platform records (Haq and Al-Qahtani, 2005). The compiled Ceno-Mesozoic and Paleozoic eustatic curves (Phanerozoic, 0 to 542 Ma) were recalibrated to recently updated geological timescale (Gradstein et al., 2020, Fig. 1A).

Variations in Earth's interior processes can be inferred from data modeling of mid-ocean spreading and plate subduction processes. Well-constrained plate tectonic and carbon cycle models of the Meso-Cenozoic interval have been constructed (e.g., Müller et al., 2016; Müller and Dutkiewicz, 2018). Cyclicities of tens of Myr were detected in these models. In particular, spectral analysis of spreading rate data detects a main cyclicity of 25 to 26 Myr (e.g., Cogné and Humler, 2006; Müller and Dutkiewicz, 2018). Here we have focused on cyclicities of tens of Myr in both spreading and subduction data for potential correlations with sea-level data. We used tectonic data of the most recent global plate model of Müller et al. (2019) that is updated from the earlier model of Müller et al. (2016). This newer model additionally includes plate deformation along major rifts and orogens since rifting of Pangea started in the Early Triassic (240 Ma). It also considers the evolution of the age-area distribution of ocean floor. This model provides mid-ocean spreading and plate subduction data as well as the total variations in the crustal production and destruction rates through time. We have also analyzed the equivalent data of the previous model (Müller et al., 2016) to see to what extent the cyclicities we find are affected by the differences in plate tectonic models.

2.2. Astronomical data

An important feature of the Earth's orbital parameter variations is that they display modulations in amplitude and frequency. The significance of certain amplitude modulation cycles was first described by Laskar (Laskar, 1990, 1999; Laskar et al., 1993), and an extensive review was later presented by Hinnov (2000). The most well known long-period modulation cycles are those of eccentricity (~2.4 Myr) and obliquity (~1.2 Myr).

Lower-frequency orbital variations (e.g., 2.4 and 4.7 Myr) are characterized by lower amplitudes when compared to higher-frequency variations (e.g., Laskar et al., 2004). However, several studies have shown strong expression of long-period orbital cycles in the sedimentary record (e.g., Beaufort, 1994; Zachos et al., 2001; Pälike et al., 2006; Mitchell et al., 2008; Boulila et al., 2010, 2011, 2012, 2014, 2020; Huang et al., 2010; Sprovieri et al., 2013; Boulila, 2019). Energy-transfer process from higher to lower astronomical frequencies is also a common feature in the sedimentary record (Boulila et al., 2012; Li et al., 2018). Our strategy for the extraction of low-frequency orbital amplitude modulation envelopes was based on choice of the strongest eccentricity (405 kyr, g₂–g₅, where g₂ and g₅ are related to the precession of the perihelions of Venus and Jupiter) and its surrounding terms, the interference of which would produce longer terms of 2.4, 4.7 and 9.5 Myr (Boulila et al., 2012, 2020; Boulila, 2019). Subsequently we bandpass filtered the 9.5 Myr band from these 400 kyr amplitude modulation envelopes for eventual, serial modulation by even longer eccentricity terms. The phase of the 9.5 Myr cycle band was rectified for correlation with sea-level data (Section 3.3). We used all available

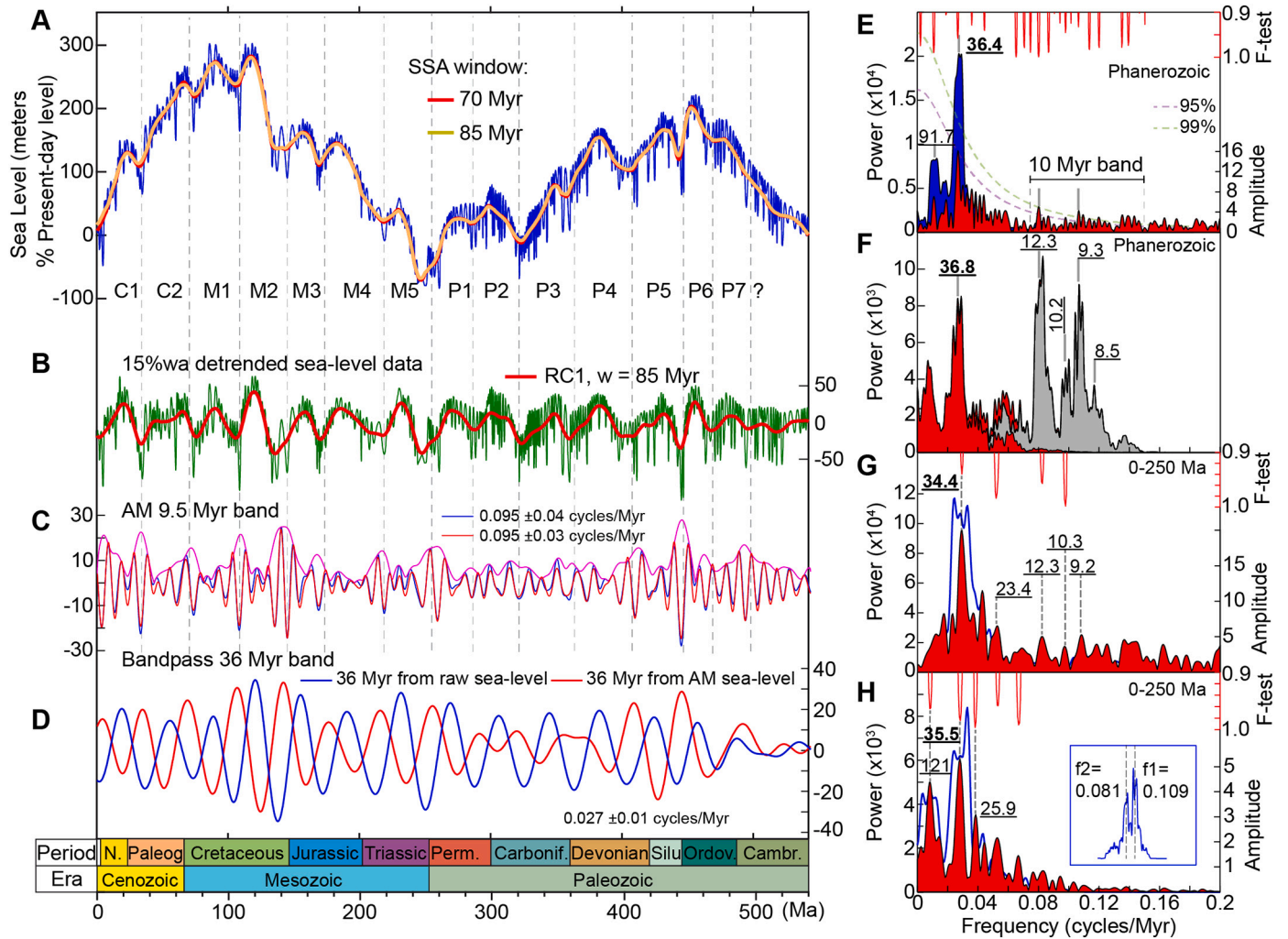


Fig. 1. Amplitude modulation analysis of Phanerozoic sea-level data. (A) Raw sea-level data (detail on reference sources is provided in Section 2.1), along with SSA lowpass filtering (RC1 with different windows indicated). (B) Detrended Phanerozoic sea-level data (Wilson cycles removed, 15% weighted average removed), along with SSA RC1. (C) 10 Myr bandpass filtering and amplitude modulation envelopes of the detrended sea-level data in 'A'. (D) 35 Myr bandpass filtering from sea-level data in 'A', and from amplitude modulation envelopes in 'B'. (E) Power and amplitude spectra of the detrended Phanerozoic sea-level data. (F) Power spectra of 10 Myr bandpass filtered (0.095 ± 0.04 cycles/Myr) sea-level data in grey and of its amplitude modulation envelope curve in red. (G) Power and amplitude spectra of the detrended sea-level data over the interval 0–250 Ma. (H) Power and amplitude spectra of sea-level amplitude modulation envelope curve of the 10 Myr band (0.095 ± 0.04 cycles/Myr) for the interval 0–250 Ma. *Inset:* Power spectrum of the 10 Myr bandpass filtered data to show the two beating frequencies $f_1 = 0.081$ (12.3 Myr) and $f_2 = 0.109$ (9.2 Myr) that produce the 35 Myr cycle. Results on the interval 0–250 Ma are shown for comparison with the astronomical data (Figs. 7 and 8). The antiphase relationship between the 35 Myr cycle from 10 Myr amplitude modulation band and that from the original data in 'D' is explained in Section 3.2. (For interpretation of the references to colour in this figure legend, the reader is referred to the web version of this article.)

astronomical data, which cover the past 250 Ma: the La2004 model (Laskar et al., 2004), and La2010a,b,c and d models (Laskar et al., 2011). Only La2004 and La2010d data show coherent cyclicities with sea-level data, and therefore only their respective amplitude modulation results were shown (Section 3.3). The robustness of La2010d with respect to other La2010 versions has already been demonstrated via a correlation with carbon-cycle data (Boulila et al., 2012). A persuasive correlation at the 9.5 Myr cycle band between carbon-cycle and La2004 astronomical data was also shown for the past 60 Ma (Boulila et al., 2012 their Fig. 1).

2.3. Time-series analysis

The Phanerozoic sea-level data are influenced by long-term Wilson megacycles, which were measured and subtracted by a 15% weighted average of the series (Fig. 1A,B). Following this detrending, the data were analyzed via the Thomson's multitaper spectral method (MTM, Thomson, 1982) with three windows, together with the harmonic F-test and the classical red noise, as implemented in the *Acycle* freeware

packages (Li et al., 2019). We conjointly used MTM amplitude (i.e., harmonic) and power spectra since the harmonic analysis allows a fine frequency decomposition, while the power spectra would average frequencies (e.g., Ghil et al., 2002). For cross-spectral analysis and correlations, we used the cross-MTM method in the Matlab routine of Peter Huybers (e.g., Huybers and Denton, 2008).

Furthermore, we perform an exploratory search for periodicities with new methods. We compute the phase distance correlation periodogram (PDCP, Zucker, 2018), which searches for periodicities without assumptions on the shape of the periodic signal, through a measurement of statistical independence between the data and an angle varying with a certain frequency. The data is phase-folded at the detected periodic features, and the shape of the periodic signals is approximated with a fitted low-order polynomial with a derivability constraint. The estimated periodic signal is then subtracted from the data and the PDCP is applied to the residuals, this procedure is repeated in an iterative manner. We further explore the fitting of non strictly periodic signals through orthonormal polynomials and Gaussian processes (Rasmussen

and Williams, 2006) with quasi-periodic kernels.

We focused on both ~ 10 and ~ 35 Myr cyclicities (Boulila et al., 2018), in particular on their potential physical (modulation) link (Fig. 1C–H). To this end, we extracted amplitude envelopes of the 10 Myr cycle band looking for the 35 Myr modulator cyclicity. We applied this approach in three steps: (1) we first bandpass filtered the 10 Myr-scale spectral peaks detected in the raw data (0.11 ± 0.04 cycles/Myr), using a Gaussian filter (Paillard et al., 1996), (2) then we applied a Hilbert transform to the filtered time series to extract the amplitude envelopes, (3) finally we compared the recovered amplitude envelopes with low-frequency variations in the raw data. For textural simplification, we refer to the above three steps as amplitude modulation analysis (see for e.g., Hinnov, 2000; Boulila et al., 2012). The illustrations of such method can be seen in Figs. 10 and 11. The 40 kyr obliquity cycle band (black curve in Fig. 10B) is modulated in amplitude by the 1.2 Myr cycle (red curve in Fig. 10B). The 100 kyr eccentricity cycle band (blue curve in Fig. 11B) is modulated in amplitude by the 400 kyr cycle (green curve in Fig. 11B), and the 400 kyr eccentricity cycle band (black curve in Fig. 11C) is modulated in amplitude by the 2.4 Myr cycle (red curve in Fig. 11C).

Lowpass filtering was performed using the Singular Spectrum Analysis (SSA) method (Ghil et al., 2002). SSA method separates signals from noise in a sequence of signal components (reconstructed components, RCs, e.g., Fig. 1A,B) that are statistically independent, at zero lag, and based on signal strength (variance).

3. Results

3.1. Time-series analysis of Phanerozoic sea-level data

Spectral analysis of Phanerozoic sea-level data shows five significant peaks of ~ 92 , ~ 37 , ~ 17 , ~ 12.3 and ~ 9.3 Myr (Figs. 1E,F and 2). The 92 and 37 Myr peaks were statistically highlighted in Boulila et al. (2018). The 17 Myr peak was discussed in Boulila (2019) and Boulila et al. (2020) in potential eccentricity terms. However, the 12.3 and 9.3 Myr in Phanerozoic sea-level data were not been examined in depth by Boulila et al. (2018). Here we show that the beating of 9.3 and 12.3 Myr frequencies may produce the 37 Myr cycle (Fig. 1C,F). Amplitude modulation output of the 10 Myr cycle band shows a dominant spectral peak of 36.8 Myr (Fig. 1F), which is very close to the 36.4 Myr peak detected in the original sea-level data (Fig. 1E). This result was further supported by independent geological data from the Canadian Basin where the variations of the duration of 10 Myr sedimentary sequences are modulated by the 37 Myr cyclicity (see below). Hereafter we refer to the ~ 37 Myr periodicity, which is the mean period over much of the Phanerozoic Eon (Fig. 2), as the 35 Myr cycle, and the shorter periods of 9.3 and 12.3 Myr as the 10 Myr cyclicity.

Correlation of the 35 Myr amplitude modulation envelopes of the 10 Myr band with 35 Myr cyclicity extracted directly from the original sea-level data show a strong coherence (Fig. 1D). Such correlation points to a physical link between the 10 and 35 Myr cyclicities, and implies that they could have a common causal mechanism (see Section 3.3).

The exploratory statistical search also yields detection of ~ 92 and 35 Myr periodicities with evidence of non-strict periodic behavior. We also found signals at ~ 17 , ~ 12.3 , ~ 9.3 Myr, as well as ~ 2.56 Myr (Supplementary Information).

Although potential uncertainties in the timescales (e.g. in the Triassic, see Haq, 2018) preclude the application of the frequency modulation method, examination of durations of shorter second-order sea-level sequences (e.g., Haq et al., 1987; Boulila et al., 2018) through time provides some evidence for frequency modulation of the 10 Myr cycle band by the 35 Myr cyclicity (Fig. 3). Spectral analysis of variations of the 10 Myr periodicity through time detects a spectral peak of 36.3 Myr, which is very close to that detected in the raw sea-level data (Fig. 3A).

This frequency modulation result is further supported by

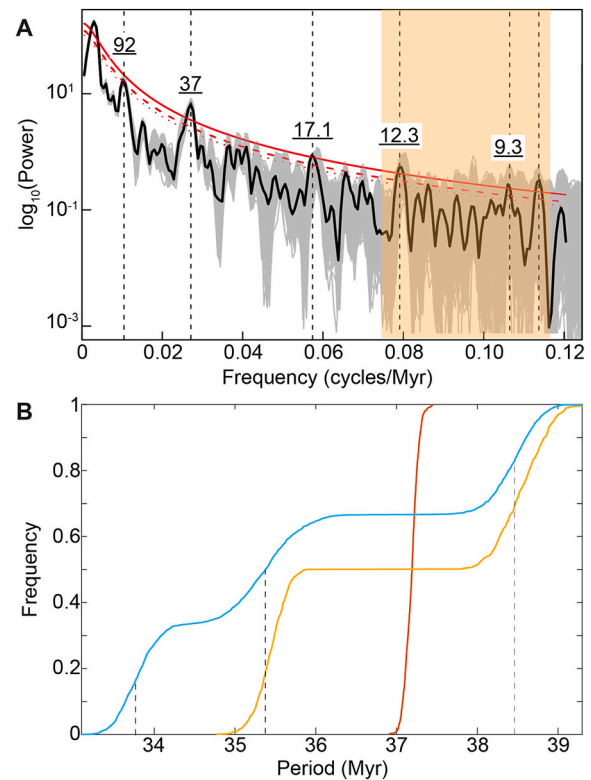


Fig. 2. Power spectra of Phanerozoic sea-level data, and quantification of the 37 Myr cyclicity per intervals (from Boulila et al., 2018). (A) Power spectrum of the raw sea-level data and confidence levels of 90%, 95% and 99%. Grey-colored spectra are 1000 Markov Chain Monte Carlo (MCMC) simulations to test the impact of timescales on the recorded periods. Light orange shaded interval indicates the 10 Myr cycle band. (B) Experimental cumulative distribution function of the 37 Myr period of sea-level data over three time intervals: the entire sea-level data, sea-level data split into two equal time intervals, sea-level data split into three equal time intervals.

independent sea-level data from the Canadian High Arctic Basin. Time-series analysis of variations of the duration of the major Canadian 10 Myr sedimentary (sea-level) sequences through time (Embry et al., 2019) faithfully captures a cyclicity of 35 Myr, matching the eustatic cycle of the reference chart (Supplementary Fig. S1). Such cyclicity in the Canadian sea-level data has been extensively studied by Rampino and Caldeira (2020) using other methods of spectral analysis. The detection of the 35 Myr periodicity in the variations of duration/frequency of the 10 Myr cycles (Fig. 3B) from the Canadian and reference sea-level data provides additional evidence that the 35 Myr cyclicity modulates the 10 Myr cycles.

3.2. Time-series analysis of geodynamic data

Spectral analysis of subduction data reveals that the 35 Myr cycle that spans much of the time series (Fig. 4). Another apparently significant peak is centred on a period of ~ 26 Myr. However, this peak disappears when we exclude the ~ 95 – 158 Ma interval from the time series, thus negating the regularity and significance of a 26 Myr cyclicity in subduction data. This result is reinforced by visual inspection and filtering of the subduction time series, where the 26 Myr bandpass filter does not match the original data (Supplementary Fig. S20).

Spectral analysis of data for crustal production rates along mid-ocean ridges (the product of seafloor spreading rates and ridge length) also shows the two peaks of 26 and 35 Myr (Fig. 4). The 26 Myr is more regular and continuously recorded. However, the 35 Myr trends are intermittently recorded. Thus, the 35 Myr is a dominant cyclicity in the

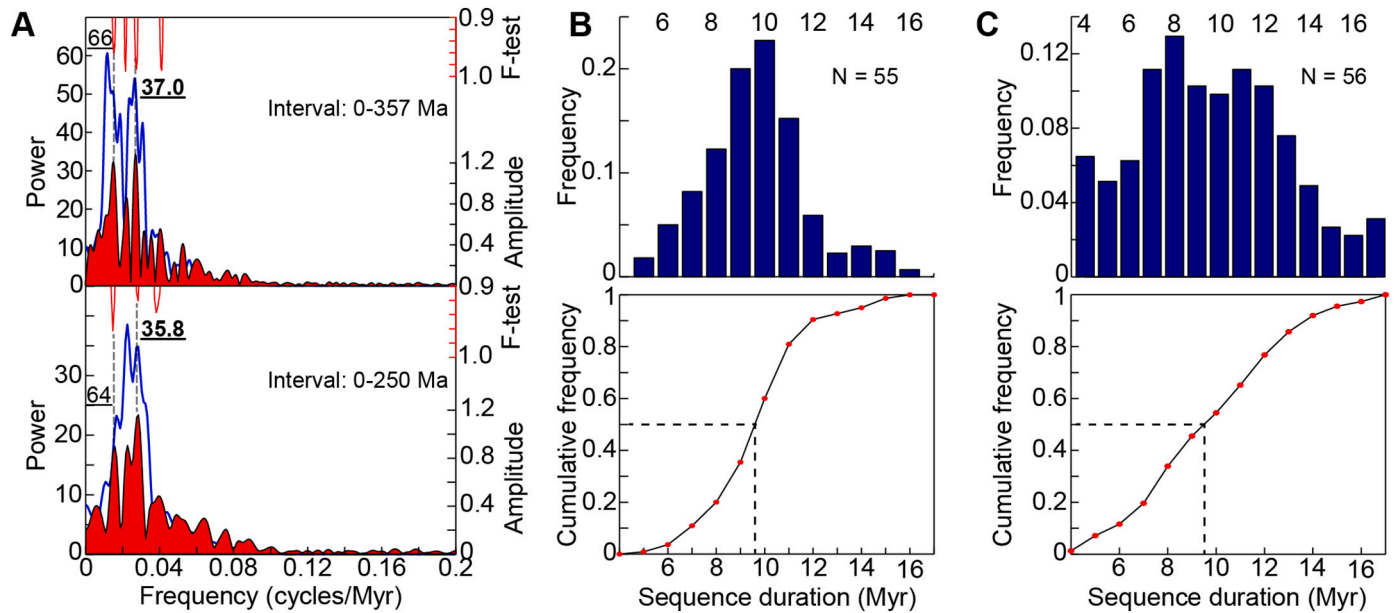


Fig. 3. Power spectra and statistics of the duration of 10 Myr scale eustatic cycles (medium-1 s-order sequences, Boulila et al., 2018, see Table 1). (A) Power spectra of the evolution of duration of 10 Myr eustatic sequences through time (data are from the sea-level reference chart, see Section 2.1 for the original references). (B) Histogram and cumulative distribution function of the duration of 10 Myr scale cycles from the reference eustatic curve. (C) Histogram and cumulative distribution function of the duration of 10 Myr scale cycles from the Canadian sequences (data are from Embry et al., 2019, see Supplementary Fig. S1). For comparison between histograms of the reference and Canadian sea-level data, durations of the reference sequences were rounded to 1 Myr as for the Canadian sequences.

subduction data (this study), while the 26 Myr is dominant in the spreading data. Cross spectral analysis of subduction and spreading data (not shown) provides no coherence, neither at the 26 Myr nor at the 35 Myr bands.

Spectral analysis of crustal production and crustal destruction rate data (Fig. 5) further supports the above results. The 26 Myr cycle is well expressed in the crustal production rate data, and somewhat in the crustal destruction rates. The 35 Myr cycle is highly coherent between crustal production and crustal destruction datasets. Additionally, the crustal destruction data exhibit higher-frequency cyclicity of ~ 14 Myr focused mainly within the interval ca. 0–90 Ma. Nevertheless, the statistical F-test fails in the detection of the 26 and 35 Myr in the crustal destruction data, pointing to the non-cyclic nature of subduction rate variations and/or because of the detected cyclicities do not span the entire time series, such as the above mentioned ~ 14 Myr cyclicity. The exploratory statistical search also yields detection of the ~ 35 Myr periodicity in subduction and crustal production data (Supplementary Information).

In summary, the 35 Myr periodicity is particularly well expressed in the global subduction rate data (Fig. 4), indicating that this cyclicity may originate from the episodicity in slab rollback and advance. Some supporting evidence for this connection is found in 2D numerical subduction models that have revealed slab rollback/advance periodicities of ~ 30 Myr (Čížková and Bina, 2015). This process would involve profound rhythmic changes in subduction deepwater cycling, and thus could explain the 35 Myr sea-level cyclicity inferred from the sedimentary record (see Discussion). The potential impact of deep mantle water recycling on sea-level oscillations has been pointed out by Cloetingh and Haq (2015) and Karlsen et al. (2019). Even though seafloor spreading and subduction processes ought to be coupled, the dominance of the 26 Myr cycle in spreading and 35 Myr cycle in subduction data suggests that these two operating periodicities are not tightly related. This reflects the influence of continental crustal deformation through time, changing the continental/oceanic crustal area ratio and thus modulating subduction flux.

The 26 Myr spreading cycle reflects mantle convection processes and far-field plate driving forces, while the 35 Myr subduction cycle is a

consequence of the time dependence of slab buoyancy and slab-mantle interaction, modulated by the trench-orthogonal migration of overriding plates, which partly reflects the deformation of overriding plates. We should also note, as mentioned above, that crustal production data record the two cyclic components of 26 and 35 Myr. The 26 Myr periodicity is potentially intrinsic to spreading processes, while the 35 Myr periodicity may reflect a dependent component to subduction processes.

Finally, detailed time-series analysis of the geodynamic data of the previous model (Müller et al., 2016) further supports the existence of a dominant 26 Myr cyclicity in seafloor spreading data and a 35 Myr cyclicity in subduction data (Supplementary Information). Additionally, we have noted short-term oscillations of a periodicity around 10 Myr in both spreading and subduction data (Supplementary Figs. 16B and S17B).

3.3. Time-series analysis of astronomical (Milankovitch) data

We tested amplitude modulation of the 10 Myr eccentricity band in all available astronomical models covering the past 250 Myr. Only La2004 and La2010d models reveal the 35 Myr cycle (Figs. 6 and 7). Amplitude modulation output of La2004 model shows a dominant spectral peak centred on the period of 34.5 Myr (Fig. 7A). Amplitude modulation output of La2010d model detects a broader peak centered on 35.6 Myr, including two main periods of 29.4 and 45.4 Myr in the amplitude spectra, averaging the 35.6 Myr period (Fig. 7A). The ~ 35 Myr spectral peak persists even when considering different analyzed time intervals or different passbands (Fig. 7A). Thus, amplitude modulation analysis of Earth's orbital eccentricity variations indicate the modulation of the ~ 10 Myr cycles by the ~ 35 cyclicity.

Increasing evidence for ~ 10 Myr orbital (Milankovitch) pacing of sea-level change and other geological processes, and the amplitude modulation relationship between the 10 and 35 Myr bands detected in sea-level record (Sections 3.1 and 4.1) and herein Milankovitch data, further supports the link between geological and Milankovitch variations at these longer timescales. Spectral analysis and amplitude modulation results of the equivalent time interval (i.e., 0–250 Ma) in the sea-level record highlight a close periodicity of 35 Myr (Fig. 1G,H). A strong

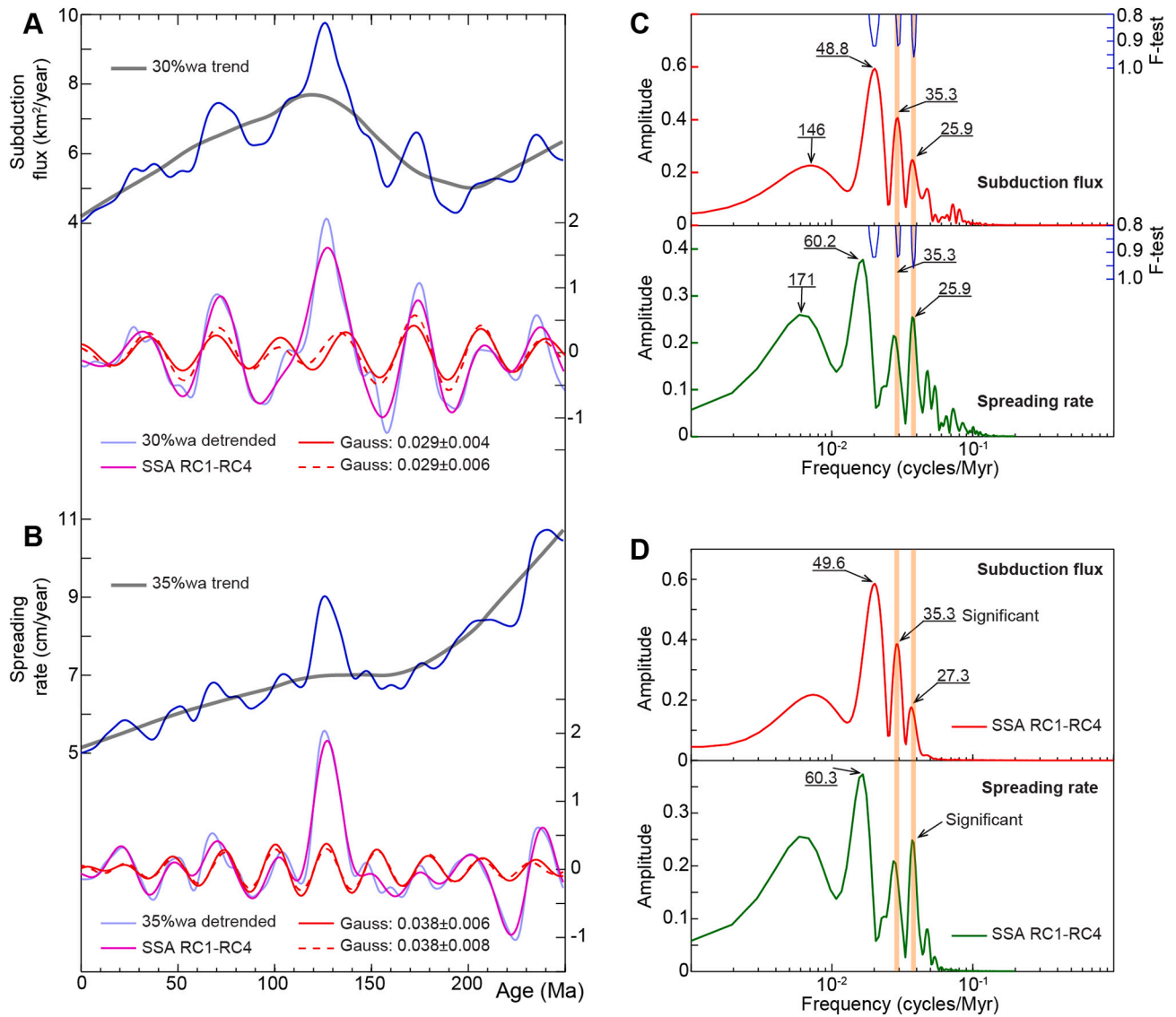


Fig. 4. Time-series analysis of plate subduction and mid-ocean spreading data of Müller et al.'s (2019) model. (A) Raw specific subduction flux, i.e., plate surface displacement per time unit (blue curve) along with weighted average (wa) smoothing (grey curve) used to detrend the raw data shown below with similar colour codes, along with SSA first components RCs (pink curve) and a 35 Myr bandpass filter (in cycles/Myr) depicted in bold and dashed red lines. Note that 35 Myr filter outputs strongly fit most of the time series, one exception is the interval of ca. 85–140 Ma, where a ~50 Myr trend overwhelmingly dominates this interval (detected by the 48.8 Myr peak). (B) Raw seafloor spreading data (blue curve) along with weighted average (wa) smoothing (grey curve) used to detrend the raw data shown below with similar colour codes, along with SSA first components RCs (pink curve) and a 26 Myr bandpass filter (in cycles/Myr) depicted in bold and dashed red lines. Note that 26 Myr filter outputs strongly fit the raw data for the interval ca. 0–175 Ma, beyond there is no record of the 26 Myr cycle, instead there is a shorter cyclicity of 21 Myr. (C) 2π -MTM spectra of detrended subduction flux (upper panel) and mid-ocean spreading data (lower panel) showing a stronger 35 Myr peak in subduction and a stronger 26 Myr peak in spreading data (indicated by light, orange-colored vertical bars). (D) 2π -MTM spectra of lowpass SSA filter outputs (RC1 through RC4 of detrended data) of subduction flux (upper panel) and spreading data (lower panel). Visual inspection and filtering highlights the dominance of 26 Myr cycle in spreading data, and the 35 Myr cycle in subduction data (Supplementary Fig. S20). (For interpretation of the references to colour in this figure legend, the reader is referred to the web version of this article.)

correlation between sea level and astronomical variations at the 10 and 35 Myr bands (Fig. 6C,E,F) provides a compelling evidence for a link between the two.

The seeming antiphase relationship between sea-level and astronomical variations at the 10 Myr band (Fig. 6C,E,F) is related to the inverted phase of the ~10 Myr orbital cyclicity due to its extraction from 400 kyr amplitude modulation envelopes (Fig. 8A,C). This feature is analogous to the 2.4 Myr cyclicity extracted from amplitude modulation of the 400 kyr band, which is characterized by an inverted phase with respect to the fundamental 2.4 Myr component in the raw eccentricity (Fig. 9, see also Laskar et al., 2011 for more detail about the corrected phase of the 2.4 Myr band). Accordingly, the actual phase of the ~10

Myr orbital cycle should be rectified (inverted) for correlation with sea-level data.

The 35 Myr amplitude modulation envelopes in the eccentricity and that in sea-level data have the same phase (Fig. 6E,F), implying an identical amplitude modulation relationship between the 10 and 35 Myr cyclicities, analogous to the 2.4 Myr versus ~10 Myr eccentricity modulations. The ~10 Myr cyclicity from 2.4 Myr eccentricity has the same phase as that extracted from the inverted 2.4 Myr eccentricity (Supplementary Fig. S2). Similarly, the 35 Myr cyclicity extracted from amplitude modulation of ~10 Myr cycles and that extracted from amplitude modulation of inverted ~10 Myr cycles are characterized by a similar phase.

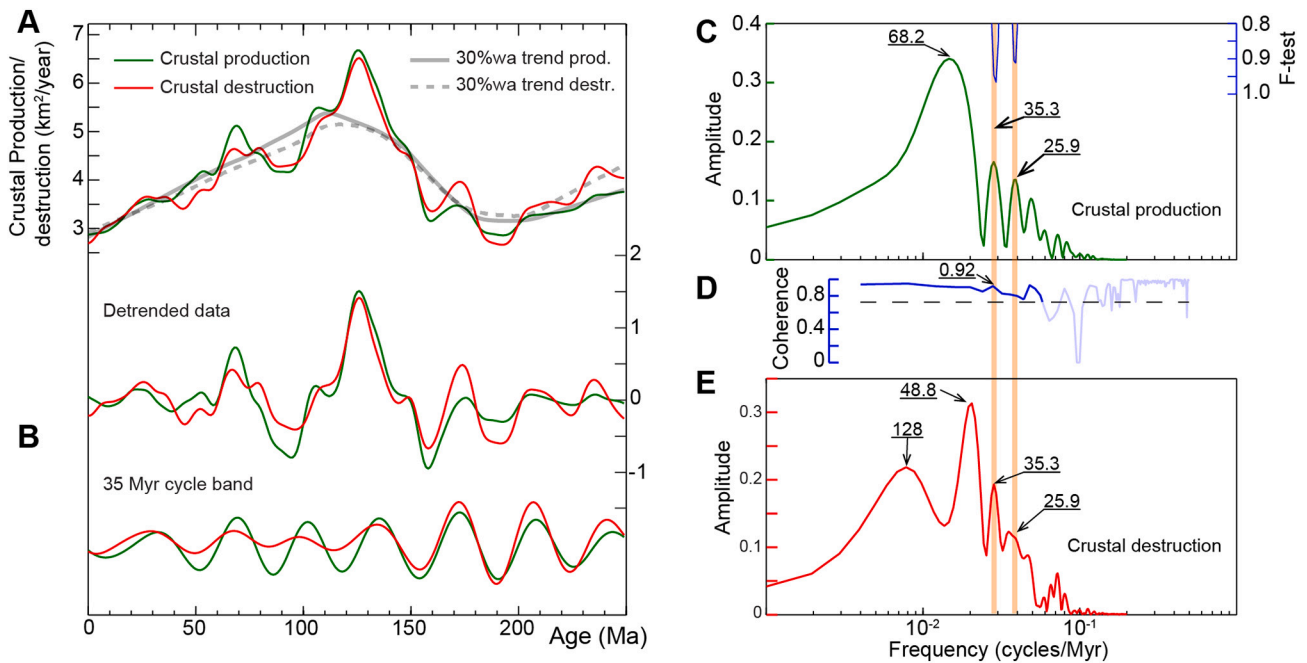


Fig. 5. Time-series analysis of crustal production and crustal destruction data of Müller et al.'s (2019) model. (A) Raw data, in green crustal production and in red crustal destruction, along with weighted average (wa) smoothed data (grey curve) showing the long-term trends. (B) Detrended data by removal of the trends shown in 'A', and 35 Myr bandpass filters (0.029 ± 0.006 cycles/Myr) using similar colour codes as in 'A'. (C) Amplitude spectrum of crustal production data. (D) Spectral coherence between crustal-production and crustal-destruction data. The higher frequency (< 20 Myr) part of the spectrum is not significant, hence we indicated it by the light colour. (E) Amplitude spectrum of crustal destruction data. (For interpretation of the references to colour in this figure legend, the reader is referred to the web version of this article.)

Thus, sea-level cyclicities share a similar phase relationship with Earth's orbital eccentricity. The 35 Myr cycle extracted directly from bandpass filtering of sea-level record is antiphased with respect to that retrieved from amplitude modulation envelopes of the 10 Myr sea-level band (Fig. 1D). This is again the same amplitude modulation physical relationship between the 400 kyr and ~ 10 Myr or between the 400 kyr and 2.4 Myr eccentricity cycles (Figs. 8 and 9, Laskar et al., 2011). In more detail, because the long-term nodes of the 400 kyr signal are a truncated function at minimal eccentricity values, which is typical for the orbital motion of a body in an eccentric trajectory. Thus, filtering of 400 kyr nodes results in amplitude modulation maxima envelopes, whereas filtering of 400 kyr maxima results in amplitude modulation minima envelopes (Fig. 9). This is different to the oscillations of the Earth's axial tilt, the values of which are not truncated at minimal (or mean) values, thus filtering of these variations retrieves the actual phase of their amplitude modulation envelopes (Fig. 10).

Sea-level data at the 35 Myr cycle band has a similar feature as that of a truncated function at minimal values. Filtering to the 10 Myr band yields 35 Myr envelopes that are in opposite of phase with respect to the 35 Myr cycles in the original data. This additional physical analogy between sea-level record and Earth's orbital eccentricity may provide additional argument for sea-level modulation by Earth's orbital eccentricity at the 35 Myr band. Minima of eccentricity corresponds to minima of sea-level and vice versa (Section 4.4).

Furthermore, the sea-level data support theoretical modeling that predicts the validity of astronomical models up to 45 Ma. Likewise, we show that the La2004 astronomical model provides the best fit with sea-level record compared to the more recent La2010d model. In particular, a good correlation between sea-level and La2004 astronomical data is not only observed up to 50 Ma at 10 Myr cycle band, but also nearly up to 150 Ma at 35 Myr cycle band, pointing to the robustness of La2004 model. The efficacy of La2004 model has already been demonstrated by correlation with other geological proxy records (carbon cycle), with a coherent phase relationship up to ~ 60 Ma (Boulila et al., 2012).

Finally, we further investigated such serial amplitude modulation of La2004 eccentricity within the most constrained time interval (0–30 Ma, Fig. 11) to seek for the multi-Myr variations and the origin of their modulating components (see also Boulila, 2019; Boulila et al., 2020). The 1.6, 2.4 and 4.7 Myr eccentricity cycles (Fig. 11E; Boulila, 2019) are associated to the resonant angle θ (Boulila et al., 2020, libration period $P\theta = 4.7$ Myr of the resonant angle θ). The 2.4 Myr cycle band presents three beating frequencies of ~ 2.1 , ~ 2.4 and ~ 2.7 Myr (Fig. 11F) providing the resulting ~ 10 and ~ 18 Myr cycles (Boulila, 2019). The 4.7 Myr cycle band shows two periods of ~ 4.3 and ~ 5.3 Myr (Fig. 11E, F), which may also provide the ~ 18 Myr cycle. The ~ 10 Myr cycle is equally detected, although the analyzed time interval is too short for such cyclicity. By analogy with well-known Milankovitch cyclicities, such as the 2.4 Myr eccentricity term, we suggest that the 10 and 35 Myr cycles may correspond to some unresolved fundamental terms, and also arise from the modulation of shorter eccentricity terms as shown in the present study.

4. Discussion

4.1. Two distinct frequency bands of tens of Myr in the geological data

Geologically detected cyclicities of tens of Myr, ranging from ca. 25 to ca. 38 Myr, have long been thought to be within the same frequency band, and differences in the detected mean periodicity are related to the quality of geological data, especially to the different timescales employed, and to the methods used for time-series analysis. However, by employing a consistent timescale for the past 240 Myr we show here that subduction data encode the 35 Myr cycle, while mid-ocean spreading data capture the 26 Myr cycle. Thus, there are two distinct frequency bands in the geological data. The mean periods of these two cyclicities could vary, depending on the analyzed time interval (see for e.g., Fig. 2B) – the mean values of these two cyclicities, over the past 200 Myr, are within the narrow ranges of ~ 25 –26 Myr and ~ 33 –35 Myr,

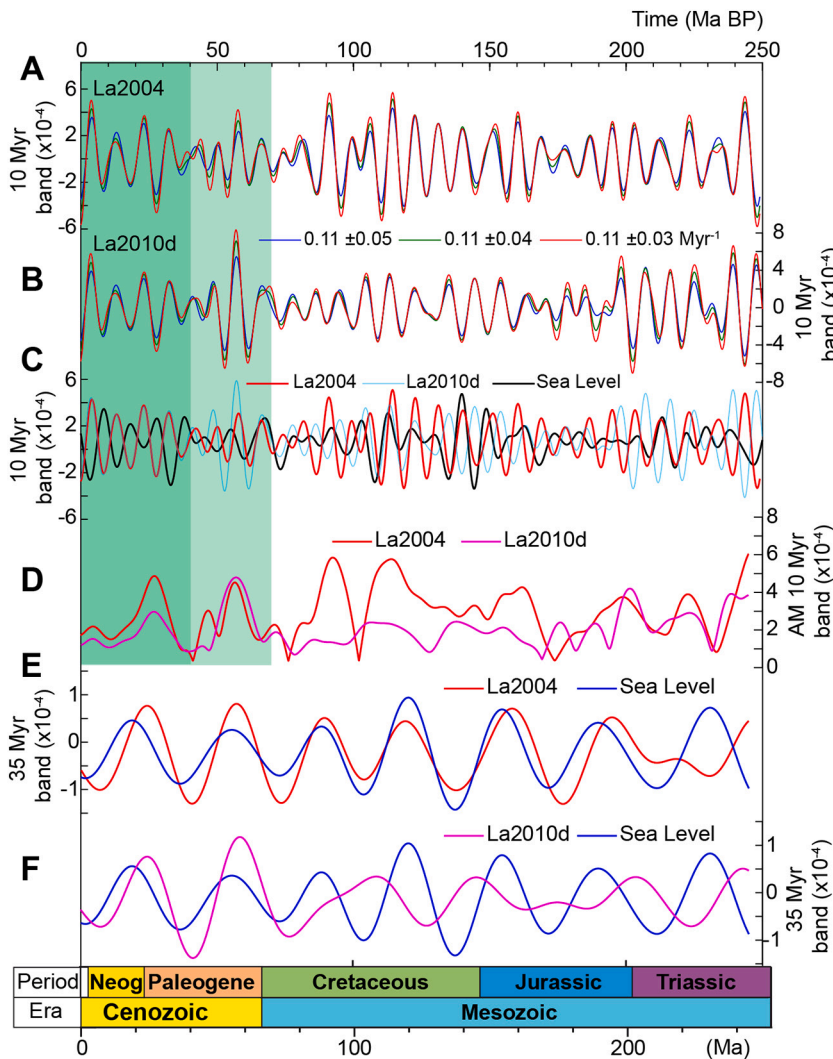


Fig. 6. Amplitude modulation analysis of the astronomical data and correlations with sea-level data at the ~10 and ~35 Myr cycle bands. (A) 9.5 Myr extracted cycles from bandpass filtered 400 kyr amplitude modulation envelopes in the La2004 model. (B) 9.5 Myr extracted cycles from bandpass filtered 400 kyr amplitude modulation envelopes in the La2010d model. (C) Correlation at the 10 Myr cycle band between sea-level, and La2004 and La2010d astronomical data. (D) Amplitude modulation envelopes of the 10 Myr band in La2004 and La2010d astronomical models. (E) Correlation at the 35 Myr cycle band between sea-level and La2004 astronomical data. (F) Correlation at the 35 Myr cycle band between sea-level and La2010d astronomical data. See Fig. 7 for the spectra of 9.5 Myr amplitude modulation envelopes in the astronomical models, and compare with spectra of sea-level data in Fig. 1G,H for the same time interval (0–250 Ma). Note the intriguing correlation between sea-level and La2004 astronomical data till nearly 150 Ma. The inverted phase of the 10 Myr cycle from 400 kyr amplitude modulation band is explained in Section 3.3.

respectively. For textural simplification, we hereafter refer to the former as the 26 Myr cycle, and to the latter as the 35 Myr cycle.

The 35 Myr cyclicity in subduction data correlates with its time equivalents in sea level, stable oxygen isotopes and Earth's orbital eccentricity (Section 4.2, Fig. 13). This cyclicity has been well documented in the geological record (reviewed in Sections 4.2 and 4.3). Also, the 26 Myr cyclicity in seafloor spreading data has previously been detected (Cogné and Humler, 2006; Müller and Dutkiewicz, 2018), and supported by our study. Indeed, the 26 Myr cyclicity has been studied since 1980s, especially in the biodiversity data of the extinction of marine families for the past 260 Myr (e.g., Raup and Sepkoski, 1984, 1988), albeit its regularity and statistical significance have been the subject of a long debate (e.g., Stigler and Wagner, 1987, 1988; Bailer-Jones, 2009). Later studies using updated biodiversity data and more recent geological timescales have further supported the existence of the 26 Myr cycle (Lieberman and Melott, 2007; Melott and Bambach, 2010, 2014; Rampino and Caldeira, 2015).

At the 26 Myr frequency band, studies have suggested a link between biomass extinction events, crater impacts and/or Earth's interior dynamics (e.g., Rampino and Stothers, 1984, 1988; Rich et al., 1986; Napier, 1988; Rampino and Caldeira, 1993; Courtillot and Renne, 2003). More recently, the 26 Myr cycle has been recorded in updated impact-cratering data, and correlated to biological extinction events over the past 260 Myr (Rampino and Caldeira, 2015). From these studies, it would seem that the 26 Myr periodicity is statistically

significant, and characteristic of mid-ocean seafloor spreading processes and the resulting flood basalt provinces, biomass extinction, and potentially also impact cratering (Rampino and Caldeira, 1993, 2015; Cogné and Humler, 2006; Rampino, 2010; Müller and Dutkiewicz, 2018). Strong evidence of flood basalt volcanism control of biomass extinctions comes from a striking correlation between CAMP eruptions and bioextinction of the end-Triassic Extinction Event (Whiteside et al., 2010). It is quite likely that the astronomical and geological events (e.g., crater impacts, bioevents, eustatic lows and highs, etc) that have been employed to look for such cyclicities of 26 and 35 Myr bands (e.g., Rampino and Caldeira, 2015) correspond to amplitude extremes of these cycles. Boulila (2019) showed that the major known climate-ocean events of the past 115 Ma strikingly match the 35 Myr extreme cycling. Further studies need to focus on time-series analysis of these cyclicities in both discrete geological events and continuous geological datasets.

4.2. The 35 Myr eustatic cycle: An historical overview

The 35 Myr cyclicity is a striking feature of the reference Phanerozoic eustatic sea-level curve based on data in Haq et al. (Haq et al., 1987; Haq and Al-Qahtani, 2005; Haq and Schutter, 2008, Fig. 1). A comparable cyclicity was already recognized in sea-level data a long time ago by Grabau (1936), who noticed several pervasive 32 Myr scale major transgressive phases during the Paleozoic (Fig. 12), which he extended

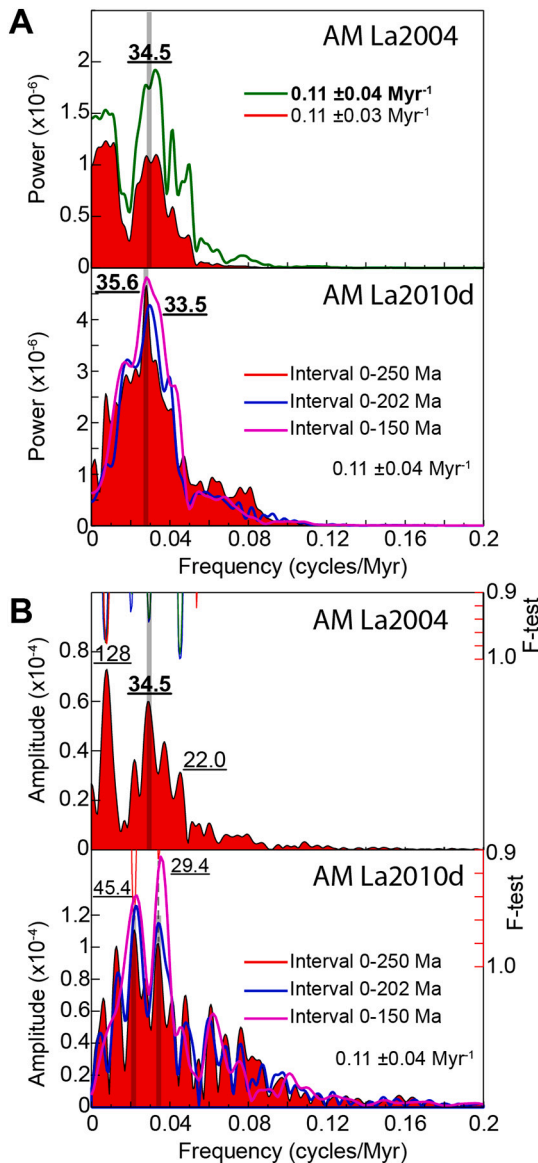


Fig. 7. Amplitude and power spectra of 10 Myr amplitude modulation envelopes in Earth's orbital eccentricity variations. (A) Power spectra. (B) Amplitude spectra. Note the high variability of the 35 Myr mean periodicity, resulting in a broad spectral peak, which is splitted into two peaks in the amplitude spectrum of La2010d model, of periods of 29.4 and 45.4 Myr averaging the 33.5 to 35.6 Myr period.

to the Phanerozoic, calling them as transgressive pulses (Grabau, 1940). Dorman (1968) suggested a 30 Myr cycle in global temperatures inferred from $\delta^{18}\text{O}$ proxy data of Cenozoic mollusks. Damon (1971) found a periodicity of about 36 Myr in Phanerozoic tectonic (magmatism) data, and correlated it to major marine transgressive-regressive phases. Wise (1974) constructed sea-level curves for the Phanerozoic, suggesting a 36 Myr periodicity for regression phases, which is identical to the period determined by Damon (1971), albeit using different sea-level datasets.

A similar 32 Myr cycle spanning the Meso-Cenozoic had then been extensively reviewed by Fischer and Arthur (1977) on the basis of sedimentological proxy data (e.g., biogenic silica, deep-sea carbonates, black shales, etc), pelagic biodiversity, and paleotemperatures and carbon-cycle derived from $\delta^{18}\text{O}$ and $\delta^{13}\text{C}$ of benthic and planktonic foraminifera. The main conclusion of these authors was that several geological processes were climatically linked to the 32 Myr cyclicity, especially the vertical and latitudinal temperature gradient (and

oxygenation) in the ocean, sea-level fluctuations, and marine biomass evolution. All these processes are sensitive to fluctuations in influx of solar energy, which modulates climate changes. Fischer and Arthur (1977) evoked two mechanisms for the 32 Myr cycle, the incident solar energy and Earth's interior processes.

The finding of the 32 Myr cycle of Fischer and Arthur (1977) in multiple geological proxy datasets is the precursor for several later studies since 1980's, that have suggested similar periodicity in the rate of extinction (Rampino and Sepkoski, 1984; Kitchell and Pena, 1984) or in the occurrence of comet showers (Davis et al., 1984; Rampino and Stothers, 1984). Rampino and Stothers (1984) inspired by the Fischer and Arthur went on to demonstrate a 33 ± 1 Myr periodicity in the Meso-Cenozoic sea-level data of Vail et al. (1977). Baker and Flood (2015) found a cyclicity of 31 Myr in Late Cretaceous to Miocene sea-level data of Kominz et al. (2008). Boulila et al. (2018) demonstrated a mean cyclicity of 36 to 37 Myr over the Phanerozoic eon based on sea-level data of Haq et al. (1987), Haq and Al-Qahtani (2005) and Haq and Schutter (2008). They have also shown that this cyclicity is shorter in the Mesozoic and Cenozoic eras, thus supporting previous estimates (e.g., Fischer and Arthur, 1977; Rampino and Stothers, 1984). They have also tested the impact of evolving geological timescales on the record of such cyclicity, and concluded the persistence of such cyclicity in global sea-level data.

In parallel, increasing stratigraphic resolution has allowed the record with high fidelity of the 35 Myr cyclicity in $\delta^{18}\text{O}$ data (Shackleton and Imbrie, 1990; Kaiho and Saito, 1994; Svensmark, 2006; Boulila et al., 2018; Boulila, 2019). The record of similar 35 Myr scale cyclicity in sea-level and $\delta^{18}\text{O}$ data (Dorman, 1968; Fischer and Arthur, 1977) reveals the climatic control of sea-level change (Fischer and Arthur, 1977; Boulila et al., 2018). However, tectonic processes are also able to force climate and sea-level changes at this timescale (e.g., Raymo et al., 1988; Lamb and Davis, 2003; Lagabriele et al., 2009; Whipple, 2009), thus the 35 Myr $\delta^{18}\text{O}$ cyclicity also reflects tectonically-driven climatic changes (Shackleton and Imbrie, 1990; Kaiho and Saito, 1994; Zachos et al., 2001).

In summary, since 1980's a number of studies have focused on the 25–40 Myr geological cyclicity and its causal mechanism in biomass extinctions, comet impacts, orogenic events, ocean anoxic events and sea-level changes. Regarding the potential drivers the views are split between the tectonic forcing hypothesis (e.g., Damon, 1971; Shackleton and Imbrie, 1990; Kaiho and Saito, 1994; Abreu et al., 1998; Bond and Grasby, 2017), and external galactic cosmic-ray or comet showers from the vertical motion of the solar system in the Milky Way galaxy (e.g., Rampino and Stothers, 1984; Rampino and Caldeira, 1993, 2015; Stothers, 1998; Svensmark, 2006, 2007; Medvedev and Melott, 2007; Randal and Reece, 2014; Baker and Flood, 2015; Rampino, 2015; Boulila et al., 2018). In Section 4.5, we propose a model that reconciles the tectonic and astroclimate (Milankovitch) hypotheses but without invoking the galactic impact (Boulila et al., 2018), unless Milankovitch (insolation) and galactic (cosmic ray) drivers are coupled (Boulila, 2019).

4.3. Evidence for the 10 and 35 Myr cyclicities in astroclimate and tectonic archives

Amplitude and frequency modulation analysis of the 10 Myr cycle band in the reference sea-level data indicates a main cyclicity of a period close to 35 Myr. This result is supported by independent data from the Canadian High Arctic Basin (Fig. 13C, Section 3.1), that record global sedimentary sequences (Embry et al., 2019, Supplementary Fig. S2). Collectively, these results provide a compelling evidence for the modulation of the 10 Myr band by the 35 Myr cyclicity in sea-level data (Figs. 13 and 14).

A number of studies have shown the existence of ~10 Myr periodicity in Milankovitch orbital variations (Boulila et al., 2012, 2020; Sprovieri et al., 2013; Boulila, 2019). The ~10 Myr orbital cyclicity can

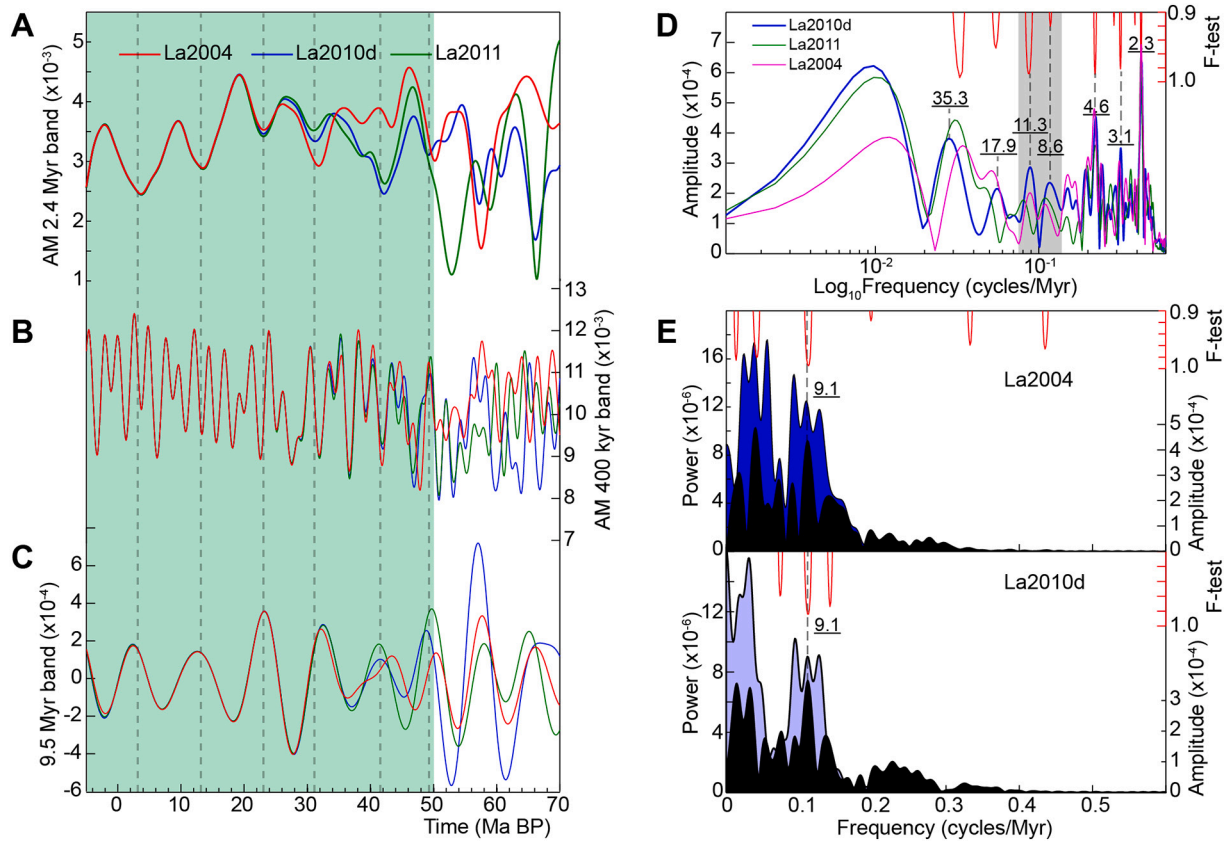


Fig. 8. Amplitude modulation analysis of the astronomical data (details on reference sources of La2004, La2010d and La2011 astronomical models are provided in Section 2.2). (A) Amplitude modulation of the 2.4 Myr cycle band, 0.43 ± 0.15 cycles/Myr (as in Boulila et al., 2012). (B) Amplitude modulation of the 400 kyr cycle band (2.465 ± 0.4 cycles/Myr). (C) Bandpass filtered 9.5 cycle band (0.11 ± 0.05 cycles/Myr) from 400 kyr amplitude modulation envelopes in 'B'. Green-dashed area roughly indicates the validity interval of astronomical data. (D) Amplitude spectra of 400 kyr amplitude modulation envelopes. (E) Amplitude and power spectra of 2.4 Myr amplitude modulation envelopes. (For interpretation of the references to colour in this figure legend, the reader is referred to the web version of this article.)

be retrieved either from the precession of perihelia or from the precession of nodes (Boulila et al., 2012, 2020; Boulila, 2019), i.e., it exists in the eccentricity and obliquity time series. Here we further support the presence of such cyclicity in Earth's orbital eccentricity, and in particular we demonstrate that it is modulated by a longer cyclicity of ~ 35 Myr. These orbitally related ~ 10 and ~ 35 Myr cyclicities have been noticed in paleoclimate proxy data, in deep-sea $\delta^{18}\text{O}$ record (Boulila, 2019).

The 35 Myr cyclicity is dominant in the subduction data (Section 3.2). However, the dominant cyclicity in spreading data is 25–26 Myr (Cogné and Humler, 2006; Müller and Dutkiewicz, 2018). The 10 Myr cyclicity is expressed in both subduction and mid-ocean spreading data (Section 3.2). Although such cyclicity should be considered with caution, our current knowledge seems to indicate that it is modulated by the 25–26 Myr cycle.

The 10 Myr cyclicity has previously also been reported from highly resolved geodynamic modeling data. A dominant 10 Myr cyclicity was detected in global intra-plate volcanism during the Cenozoic (Mjelde et al., 2010). In addition, a secondary 5 Myr cyclicity was detected in these data (Mjelde et al., 2010), which is close and potentially equivalent to the 4.7 Myr orbital cyclicity (Boulila et al., 2020). The 10 and 5 Myr tectonic cycles were attributed to global fluctuations in core-mantle interaction, involving periodic heating of the core and subsequent heat release to the mantle and increased global plume activity from the edges of the lower-mantle anomalies (Mjelde et al., 2010). A 10–15 Myr cyclicity has more recently been recorded in continental back-arc process (Wolfram et al., 2019). An extensive review of variations in global magmatic systems brought out cyclicities ranging from 5 to 10 Myr (Mitchell et al., 2019), further supporting tectonic fluctuations at these

timescales.

The 35 Myr is generally well preserved in geodynamic data because of its stronger amplitude and fewer errors on its estimate from modeling resolution and temporal uncertainties. A prominent cyclicity of 25–50 Myr has also been recognized in the western American Cordilleras (DeCelles et al., 2009). The record of 25–26 Myr in mantle convection and 35 Myr in subduction remains unresolved. We tentatively hypothesize that the interference of these two cyclicities may result in the 92 Myr cycle ($1/26 - 1/36$) seen in sea-level data (Fig. 2). The 92 Myr cycle has equally been recorded in other very long geological datasets including tectonics (Puetz and Borchardt, 2015; Puetz et al., 2018; Wiemer et al., 2018).

4.4. Driving mechanisms of Myr to multi-Myr eustatic cycles

The well-known driving mechanism of sea-level changes is glacioeustasy in icehouse periods, i.e. change in seawater volume by waxing and waning of continental ice sheets. Such mechanism would generate larger sea-level oscillations of magnitude reaching 120 to 130 m below present-day sea-level as during the Last Glacial Maximum, ca. 27 to 20 ka (e.g., Peltier and Fairbanks, 2006; Austermann et al., 2013; Miller et al., 2020). The 100 kyr Quaternary glacial cycles have an amplitude of 100–150 m of glacioeustatic change (e.g., Miller et al., 2005a; Siddall et al., 2010). Estimates from deep-sea $\delta^{18}\text{O}_{\text{benthic}}$ and backstripping suggest Myr-scale variations of 20 to 50 m driven by ice-volume variations during pre-Pliocene Cenozoic icehouses (John et al., 2004; Miller et al., 2005a, 2020).

The Earth during the Phanerozoic witnessed long-lasting greenhouse

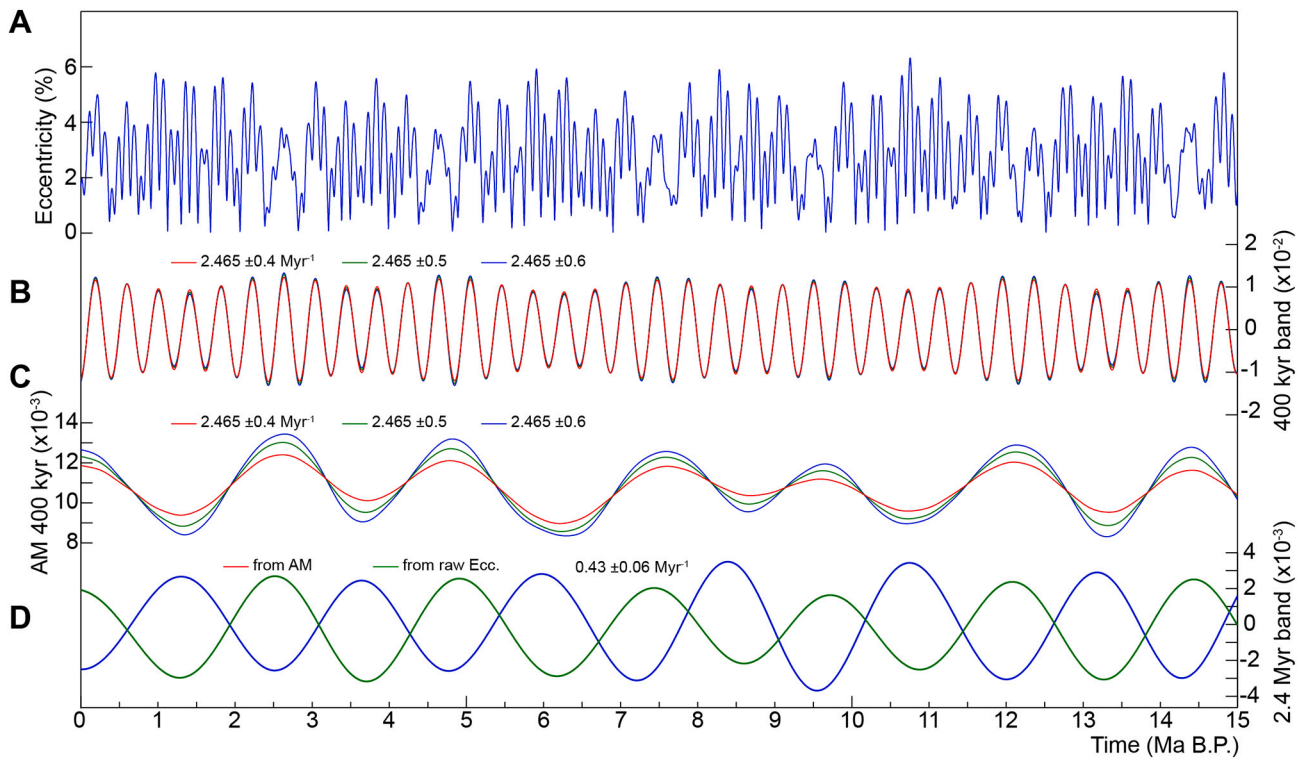


Fig. 9. 2.4 Myr eccentricity phasing. (A) La2004 raw eccentricity time series (Laskar et al., 2004). (B) 400 kyr eccentricity bandpass filtering (indicated frequency bands are in Myr^{-1}). (C) Amplitude modulation envelopes of the 400 kyr bandpass filtered time series. (D) Comparison of 2.4 Myr filtered eccentricity cyclicity ($0.43 \pm 0.06 \text{ Myr}^{-1}$) from 400 kyr amplitude modulation envelopes in 'C' and that from the original eccentricity data in 'A'.

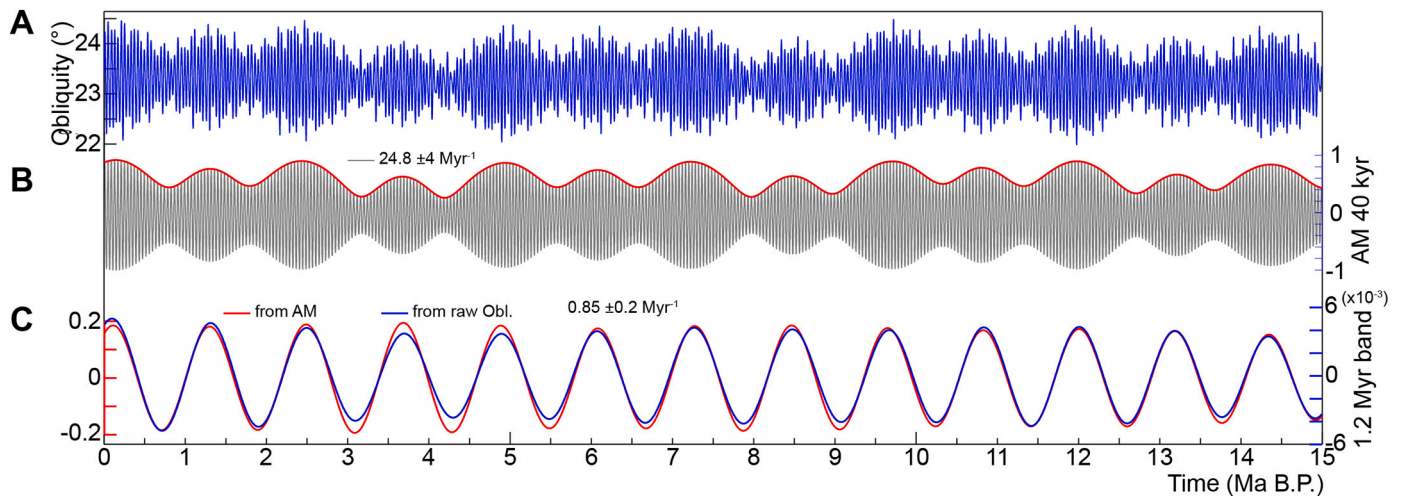
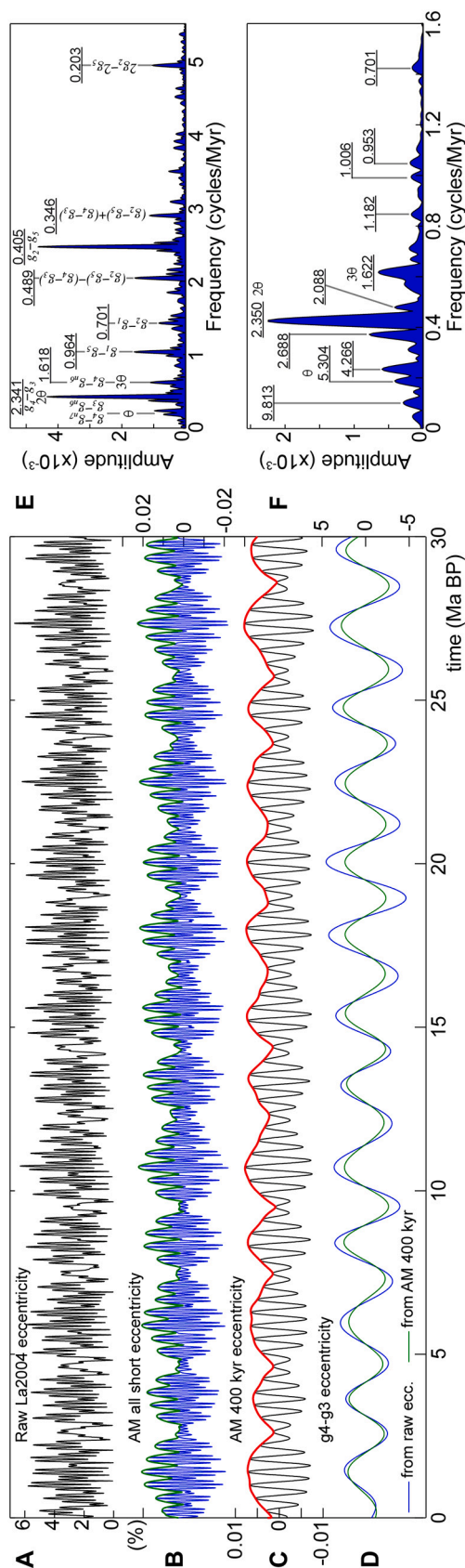


Fig. 10. 1.2 Myr obliquity phasing. (A) La2004 raw obliquity time series (Laskar et al., 2004). (B) 40 kyr bandpass filtering ($24.8 \pm 4 \text{ Myr}^{-1}$) and amplitude modulation envelopes (red curve). (C) Comparison of 1.4 Myr filtered obliquity cyclicity ($0.85 \pm 2 \text{ Myr}^{-1}$) from 40 kyr amplitude modulation envelopes in 'B' and that from the original obliquity data in 'A'. Note: a larger band in 'C' of, for example, $0.85 \pm 0.4 \text{ Myr}^{-1}$ would integrate other longer obliquity periods, such as the 799 kyr and 2.4 Myr components. Therefore, an appropriate band of $0.85 \pm 0.2 \text{ Myr}^{-1}$ is more conservative to restore the actual phase of the 1.2 Myr cyclicity. (For interpretation of the references to colour in this figure legend, the reader is referred to the web version of this article.)

periods without ice sheets or with ephemeral continental ice sheets (Miller et al., 2004, 2005b; Haq and Al-Qahtani, 2005; Royer et al., 2004; Bornemann et al., 2008; Galeotti et al., 2009; Boulila et al., 2011), against shorter icehouse periods with extended, well-developed ice sheets (Fig. 1). Glacial conditions have been episodically recorded over the Phanerozoic eon, in the Late Ordovician–Early Silurian, the Late Devonian, through much of the Carboniferous and Permian, the Late Paleogene–Neogene (e.g., Fischer, 1984; Frakes et al., 1992; Deynoux et al., 1994; Zachos et al., 2001; Haq and Schutter, 2008), and

potentially in the Late Cretaceous during the ephemeral Antarctic ice phases (Matthews, 1984; Stoll and Schrag, 1996, 2000; Miller et al., 2003, 2005b; Bornemann et al., 2008, among others). During the Mesozoic, Myr-scale sea-level cycles of a few to several tens of meters (Miller et al., 2005a; Kominz et al., 2008) have been argued to be paced by Milankovitch orbital forcing via glacioeustasy (Boulila et al., 2011). During the Paleozoic, the magnitude of shorter (Myr-scale, Boulila et al., 2011) sea-level cycles were assessed at a few tens of meters up to 125 m, the most prominent ones were related to glacioeustasy (Haq and



(caption on next column)

Fig. 11. Amplitude modulation of the orbital eccentricity. (A) La2004 raw eccentricity. (B) Amplitude modulation of the short eccentricity (bandpass: 0.009 ± 0.003 cycles/kyr). (C) Amplitude modulation of the 400 kyr eccentricity (bandpass: 0.00247 ± 0.001 cycles/kyr, applied to amplitude modulation envelopes in 'B'). (D) Bandpass (0.0004256 ± 0.002 cycles/kyr) filtered g4-g3 from amplitude modulation envelopes in 'C' (green curve) and from the raw eccentricity in 'A' (blue curve). (E) Amplitude spectrum of amplitude modulation of short eccentricity band (green curve in 'B'). (F) Amplitude spectrum of amplitude modulation of 400 kyr eccentricity band (red curve in 'C'). (For interpretation of the references to colour in this figure legend, the reader is referred to the web version of this article.)

Schutter, 2008). Although the Paleozoic sea-level sequences are in generally less precisely dated, when compared to the Ceno-Mesozoic sequences (Haq and Schutter, 2008), careful examination of several glacio-eustatic sequences points to Myr-scale sea-level sequences matching Milankovitch orbital band (Fig. 15, Boulila et al., 2011, see Supplementary information for detailed comments on Fig. 15). Some lines of evidence for icehouse conditions throughout the Earth's history have been reported, suggesting that sea-level oscillations were largely glacio-eustatically driven (Matthews, 1984; Stoll and Schrag, 1996, 2000; Abreu et al., 1998; Immenhauser, 2005; Miller et al., 2003, 2005b; Bornemann et al., 2008; Matthews and Al-Husseini, 2010; Boulila et al., 2011, among others).

The other alternative mechanism for sea-level fluctuations at Myr to multi-Myr timescales is tectono-eustasy from Earth's interior processes and plate tectonic motions. It is considered as the main candidate to explain the high-amplitude eustatic variations, especially during the so-called greenhouse periods when there were no extensive ice sheets on Earth (e.g., Vail et al., 1977; Haq et al., 1987). Tectonic processes driving sea-level and their operating timescales were recently reviewed by Conrad (2013). The main process is the change in the volume of global ridge system via mantle convection (e.g., Pitman, 1978; Harrison, 1990; Miller et al., 2005a; Cogné et al., 2006; Cogné and Humler, 2008; Müller et al., 2008; Cloetingh and Haq, 2015), which involves the creation of new ridges within the ocean basins as well as spreading rates which when accelerates tends to flatten the ridge system, raises the depth of the seafloor and elevates global sea level (Pitman, 1978; Gaffin, 1987). Global ridge-system process could account for several meters of sea-level changes in only a few Myr, to ~50 m in approximately 20 to 30 Myr, and to ~200 m at 100 to 200 Myr timescales (Conrad, 2013). At similar timescales, the production of seafloor should be compensated by subduction process, where older lithospheric plates tend to subduct to satisfy solid Earth's mass conservation – however, the average age and depth of subducting seafloor changes through time, while the age and depth of newly produced seafloor does not change. The fluctuations in the age of subducting seafloor are a reflection of the changing age-area distribution of seafloor through time (Wright et al., 2020) resulting in long-term sea level fluctuations. In addition, seawater gain from convection and seawater loss in subduction (Conrad, 2013) contributes to this process. At very long timescales (Gyr), convection and subduction processes result in an imbalance of the ocean's water exchange with the deep mantle (Conrad, 2013).

Mantle flow and the resulting upwellings and downwellings generate so-called dynamic topography at relatively long wavelengths (Gurnis, 1993; Conrad and Gurnis, 2003). This process would generate lateral and vertical motions on lands and seas, deflecting seafloor bathymetry and modifying the volume of the ocean basins (Gurnis, 1993; Conrad et al., 2004; Spasojevic and Gurnis, 2012; Flament et al., 2013; Cloetingh and Haq, 2015). The impact of dynamic topography on sea-level change is estimated to be in the range of 100–200 m since the Late Cretaceous (Conrad, 2013), and may have also played an important role in high-frequency (third- and higher orders) sea-level cycles, of up to 50 m (Lovell, 2010; Petersen et al., 2010). The vertical motions associated to the dynamic topography could also generate local uplift and subsidence patterns (e.g., Gurnis, 1993; Moucha et al., 2008; Braun, 2010;

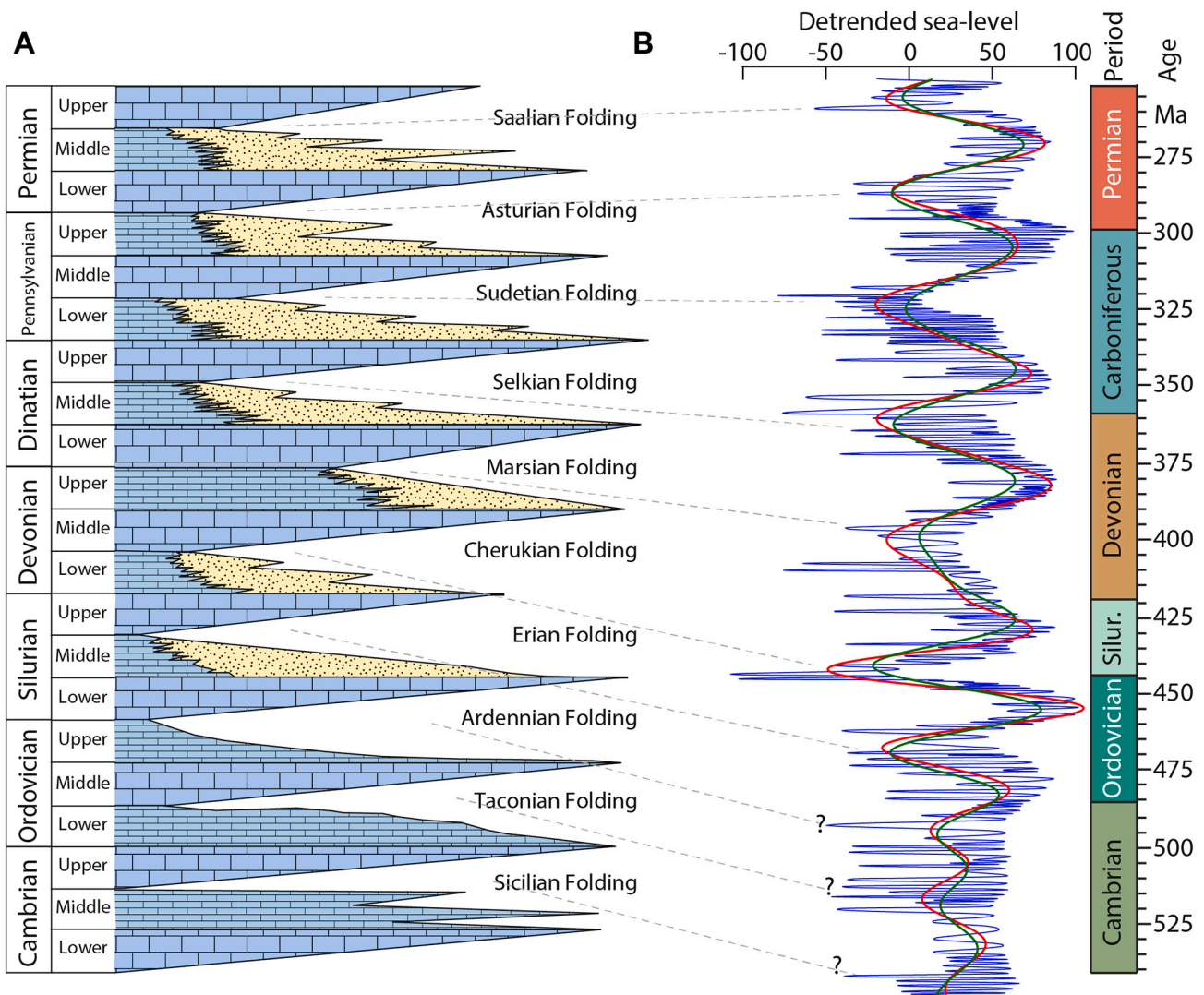


Fig. 12. Paleozoic 35 Myr eustatic cycle. (A) Major global transgressions recognized by Grabau (1936) (modified after Simmons, 2012). (B) Detrended (Wilson Magacycle removed) Paleozoic eustatic data of Haq and Schutter (2008) along with 35 Myr bandpass filtering (0.032 ± 0.01 cycles/Myr in green and 0.032 ± 0.02 cycles/Myr in red) and potential correlation with 35 Myr equivalent cycles of Grabau (1936). (For interpretation of the references to colour in this figure legend, the reader is referred to the web version of this article.)

Lovell, 2010), including those along continental margins (Müller et al., 2018), which were suggested as the main driver of second-order (10 Myr) sea-level sequences (e.g., Embry et al., 2019).

Spectral analysis of subduction data from most a recent plate tectonic models (Müller et al., 2016, 2019) shows evidence of 33 to 35 Myr cyclicity over the past 200 Myr (Fig. 13I and Supplementary File). A close cyclicity is also detected in sea-level, $\delta^{18}\text{O}$ and Milankovitch variations (Fig. 13F–J). Interestingly, cross-spectral analysis highlights a strong correlation between the subduction, sea-level, $\delta^{18}\text{O}$ and eccentricity variations at the 35 Myr cycle band (Fig. 14), suggesting a link between Earth's interior and surface processes, mediated by external Milankovitch forcing (Section 4.5). Subduction lags sea-level change by only ~ 0.5 Myr (phase = -175° at 34 Myr, coherence = 0.96, Fig. 14). Thus, higher subduction leads to lower sea levels. This would imply that the episodicity in slab advance would generate a loss in seawater (Conrad, 2013; Karlsen et al., 2019), inducing minima in the 35 Myr sea-level cycle. A potential scenario to link tectono-eustatically driven sea-level to external (Milankovitch) climate forcing of Earth's surface processes is provided below in Section 4.5. Other, relatively minor contributions to sea-level change during icehouse and greenhouse climates also need to be considered, such as the thermal expansion of seawaters

(thermo-eustasy), and terrestrial water storage and groundwater-driven eustasy called aquifer-eustasy (e.g., Jacobs and Sahagian, 1993, 1995; Lombard et al., 2005; Föllmi, 2012; Wagreich et al., 2014; Sames et al., 2016, 2020; Wendler et al., 2016; Wendler and Wendler, 2016; Ray et al., 2019; Davies et al., 2020). For instance, the impact of aquifer-eustasy on short-term (400 kyr to 3 Myr) sea-level change is increasingly advocated, especially during the Cretaceous greenhouse period (e.g., Föllmi, 2012; Sames et al., 2016; Wendler et al., 2016; Wendler and Wendler, 2016; Sames et al., 2020). Nevertheless, the larger magnitude sea-level cycles of up to 65 m assessed for the Cretaceous challenge the aquifer-eustasy hypothesis, and favor the glacio-eustasy hypothesis even during greenhouses (e.g., Miller et al., 2005b; Boulila et al., 2011; Ray et al., 2019; Davies et al., 2020; Simmons et al., 2020). The interplay of the above processes, aquifer-, glacio-, thermo-, and tectono-eustasy to sea-level change is likely (e.g., Simmons et al., 2020) at shorter and longer timescales (Section 4.5).

4.5. A coupled climate-tectonic model for the 10 and 35 Myr eustatic cycles

Astronomically forced sea-level hierarchy spans a large temporal

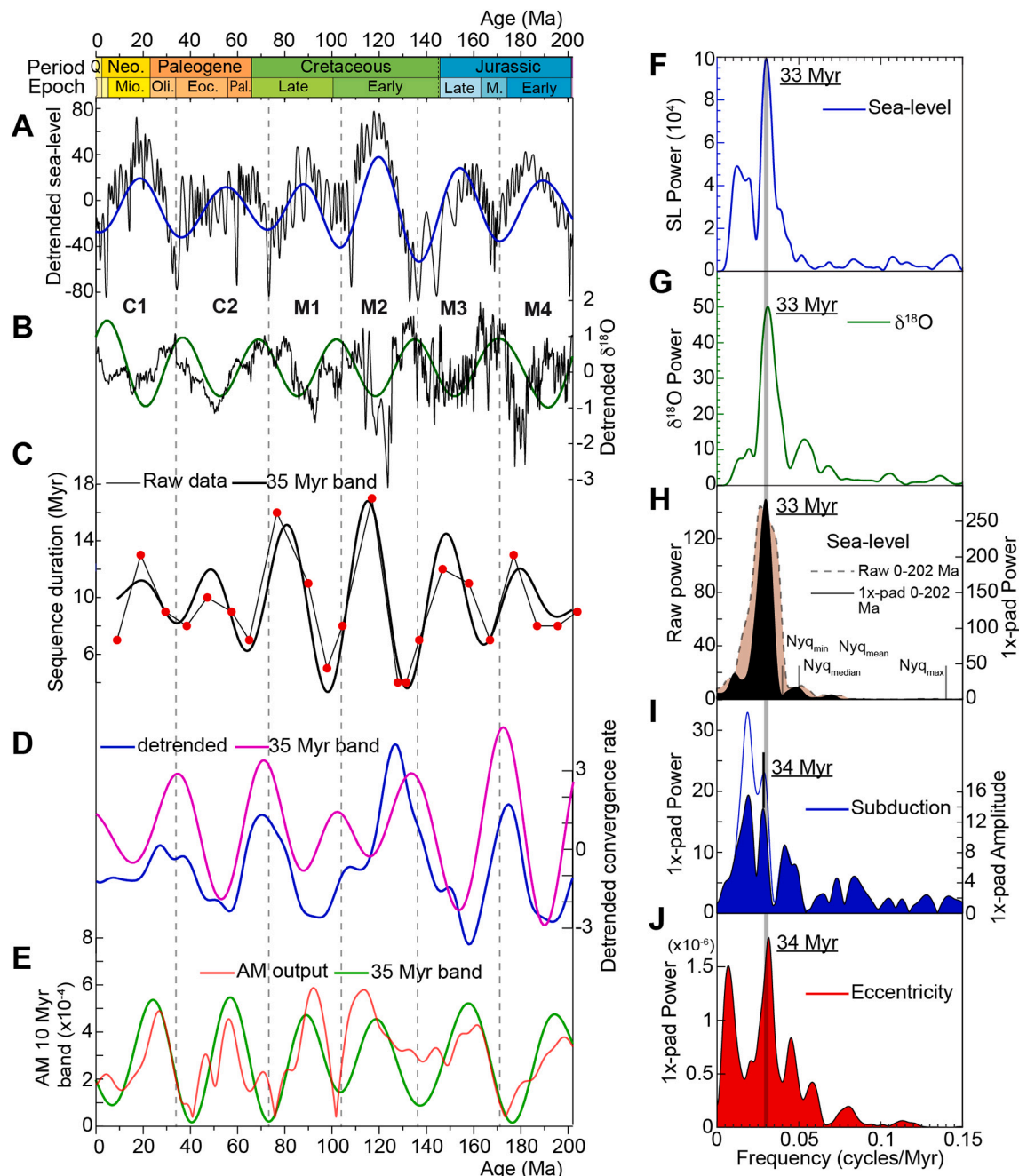


Fig. 13. Time-series analysis of four geological datasets of the past ~200 Ma to highlight the 35 Myr cyclicality. ‘A’, ‘B’, ‘F’ and ‘G’ are from [Boulila et al. \(2018\)](#). (A) Detrended eustatic reference data (Wilson megacycle removed), along with 35 Myr bandpass filtering. (B) Detrended oxygen isotope data ($\delta^{18}\text{O}$) (Wilson megacycle removed) along with 35 Myr bandpass filtering. (C) Duration of major sequence boundaries through time (black curve), from the Canadian High Arctic Basin ([Embry et al., 2019](#), see Fig. S1), and 35 Myr bandpass filtering (bold black curve). (D) Detrended convergence data of [Müller et al. \(2019\)](#) (blue, RC1, $w = 25$ Myr, step = 1 Myr) and 35 Myr bandpass filtering (pink, 0.0295 ± 0.015 cycles/Myr). (E) La2004 eccentricity amplitude modulation data (see Methods), along with a 35 Myr bandpass filtering (0.0295 ± 0.015 cycles/Myr, light green curve). (F) Power spectrum of data in ‘A’ (detrended). (G) Power spectrum of data in ‘B’. (H) Power spectra of data in ‘C’. (I) Power spectra of data in ‘D’ (see raw spectra in Fig. 4A and detail in Supplementary Fig. S15). (J) Power spectra of data in ‘E’ (see raw spectra in Supplementary Fig. S3). (For interpretation of the references to colour in this figure legend, the reader is referred to the web version of this article.)

band from millennial precession period to multi-Myr orbital modulations (Table 1). Strong evidence of a 20 kyr precession to 1.2 and 2.4 Myr orbital modulation of sea-level changes has been found throughout the Phanerozoic ([Strasser et al., 2006](#); [Boulila et al., 2011](#); [Fang et al., 2015](#); [Liu et al., 2019](#)). Longer orbital periods of 4.7 and 10 Myr have also been suggested to pace long-term geological processes including sea-level ([Boulila et al., 2012](#); [Sprovieri et al., 2013](#); [Boulila, 2019](#); [Boulila et al., 2020](#)). Our finding of 35 Myr modulation of the 10 Myr cycles in eccentricity and sea-level data further extends such a hierarchical link

between Milankovitch and sea-level cycles (Table 1). The 10 and 35 Myr periodicities have similarly been detected in tectonic data (Sections 3.2 and 4.3).

The most likely phenomenon that may link insolation-climate to Earth’s interior processes is climatically driven mass changes on Earth’s surface (e.g., [Métivier et al., 2010](#); [Rietbroek et al., 2012](#)). Thus, the potential link between external and Earth’s interior processes would manifest as interactions and feedbacks ([Boulila, 2019](#)), rather than a direct orbital forcing of the solid Earth.

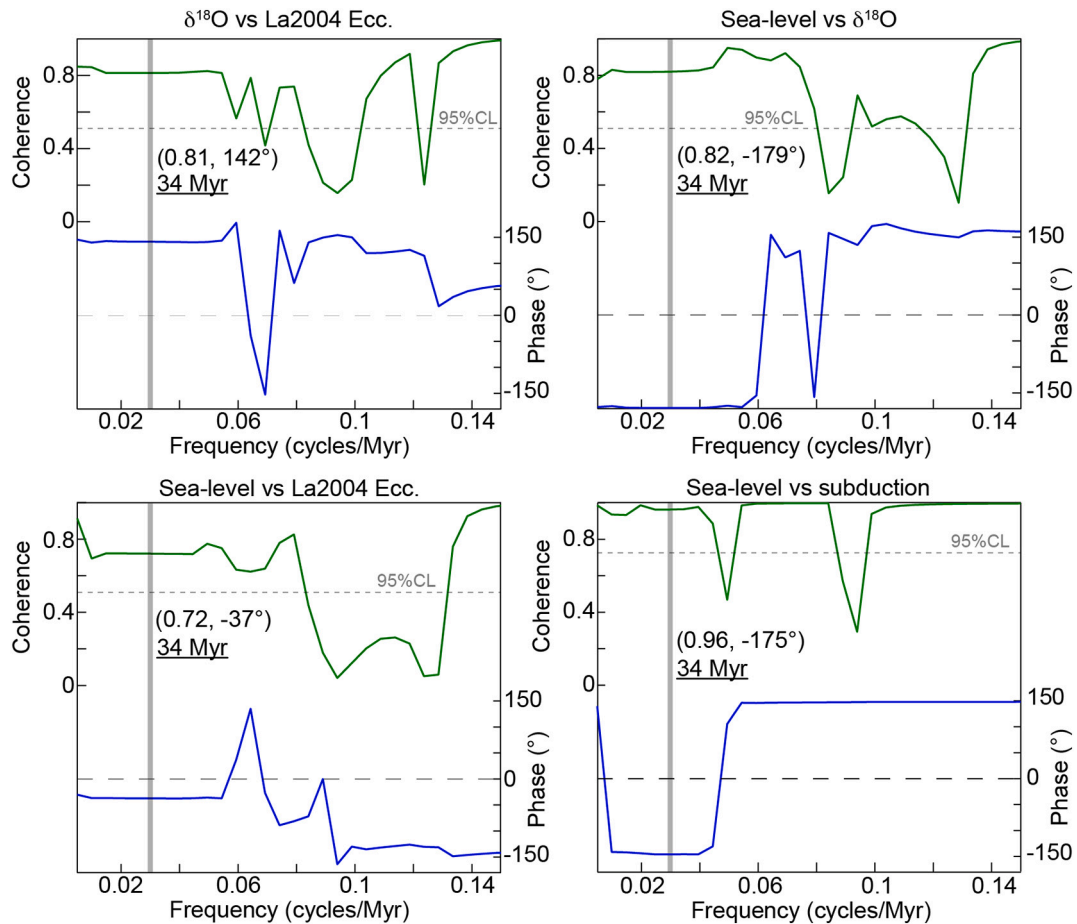


Fig. 14. Cross spectral analysis of sea-level, $\delta^{18}\text{O}$, La2004 eccentricity envelopes (La2004 Ecc.), and subduction data at the 34 Myr cycle. Coherence and phase values for each cross spectrum are given between brackets.

It has long been argued that the change in the shape of Earth's surface via the redistribution of Earth's water masses would distort the entire Earth system by displacing its barycenter (e.g., [Haskell, 1935](#); [Mitrovica and Peltier, 1993](#); [Conrad and Hager, 1997](#); [Nerem and Wahr, 2011](#); [Roy and Peltier, 2011](#)). Redistribution of water mass on Earth's surface would induce elastic and viscous deformations of the solid Earth, and these two modes of deformation deflect the seafloor as well as the gravitational equipotential (geoid) surface that defines sea-level; both processes affect relative and global sea-level, but at different timescales ([Haskell, 1935](#); [Farrell, 1972](#); [Walcott, 1972](#); [Farrell and Clark, 1976](#)). Elastic deformation operates at 1 to 100 years timescales, while the viscous deformation acts at longer timescales of 1 to 100 kyr (see [Conrad, 2013](#) for a review). Although the mechanically deformed Earth's surface due to glaciation/deglaciation could be local and over shorter timescales, such elongation is susceptible to propagate outside the deformation site, thus affecting sea-level at larger scale ([Farrell and Clark, 1976](#); [Mitrovica and Peltier, 1991](#); [Conrad, 2013](#)), and its low-frequency modulation via the hydrological cycle (e.g., [Mason et al., 2004](#)) is very likely (see below). It has even been demonstrated that seawater ocean loading causes a similar viscous response along coastlines that leads to changes in the global eustatic sea level ([Mitrovica and Milne, 2002](#)). Such a mechanism has long been recognized ([Walcott, 1972](#); [Clark et al., 1978](#); [Nakada and Lambeck, 1989](#); [Mitrovica and Peltier, 1991](#)).

These perturbations of Earth's surface from ice-mass and seawater ocean loading/unloading could be transferred to the deep solid Earth system. Observations of the match between orbitally paced Quaternary glacial cycles and global volcanic eruption has led to linkage between Earth's surface and interior processes at the orbital timescale (e.g.,

[Rampino et al., 1979](#); [McGuire et al., 1997](#); [Huybers and Langmuir, 2009, 2017](#); [Lund and Asimow, 2011](#); [Schindlbeck et al., 2018](#)). Large eruptions have been correlated to 100 kyr glacial cycles at Mount Mazama ([Bacon and Lanphere, 2006](#)), Western Europe ([Nowell et al., 2006](#)), and the South Eastern United States ([Jellinek et al., 2004](#)). It is thus suggested as a causal link between loading and removal of ice on and from continents and the resulting general perturbations of the lithosphere and upper mantle (e.g., [Nowell et al., 2006](#); [Huybers and Langmuir, 2009](#)). Orbitally-paced glacial cycles could modify the pressure exerted on the upper mantle, causing in turn the change in magma production and thus the global volcanic activity (e.g., [MacLennan et al., 2002](#); [Jellinek et al., 2004](#); [Huybers and Langmuir, 2009](#); [Kutterolf et al., 2012](#); [Crowley et al., 2015](#); [Tolstoy, 2015](#); [Conrad, 2015](#); [Schindlbeck et al., 2018](#)). In particular, [Crowley et al. \(2015\)](#) highlighted a correlation between abyssal hill fabrics along mid-ocean ridges and the glacial cycles, suggesting cyclic magmatic response to changes in sea level. In addition, at Milankovitch time scales and longer, it was postulated that magmatic variation could cause climate change via volcanic emissions of greenhouse gases, impacting in turn Earth's surface processes including sea-level changes ([Sternai et al., 2020](#)). The interplay between tectonics, climate and Earth's surface processes was also suggested to explain the evolution of mountain building ([Pesek et al., 2020](#)).

Likewise, it has been hypothesized that annual, seasonal and tidal cycles are fingerprinted in seafloor volcanic variations, suggesting that tidal to annual changes in sea-level and environments (tides) would govern deformation of Earth's surface, and thus pace the global volcanic activity (e.g., [Emter, 1997](#); [Mason et al., 2004](#); [Jupp et al., 2004](#)). Milankovitch periodic parameters (precession, obliquity and eccentricity) modulate the annual and seasonal cycles (e.g., [Berger et al., 2006](#);

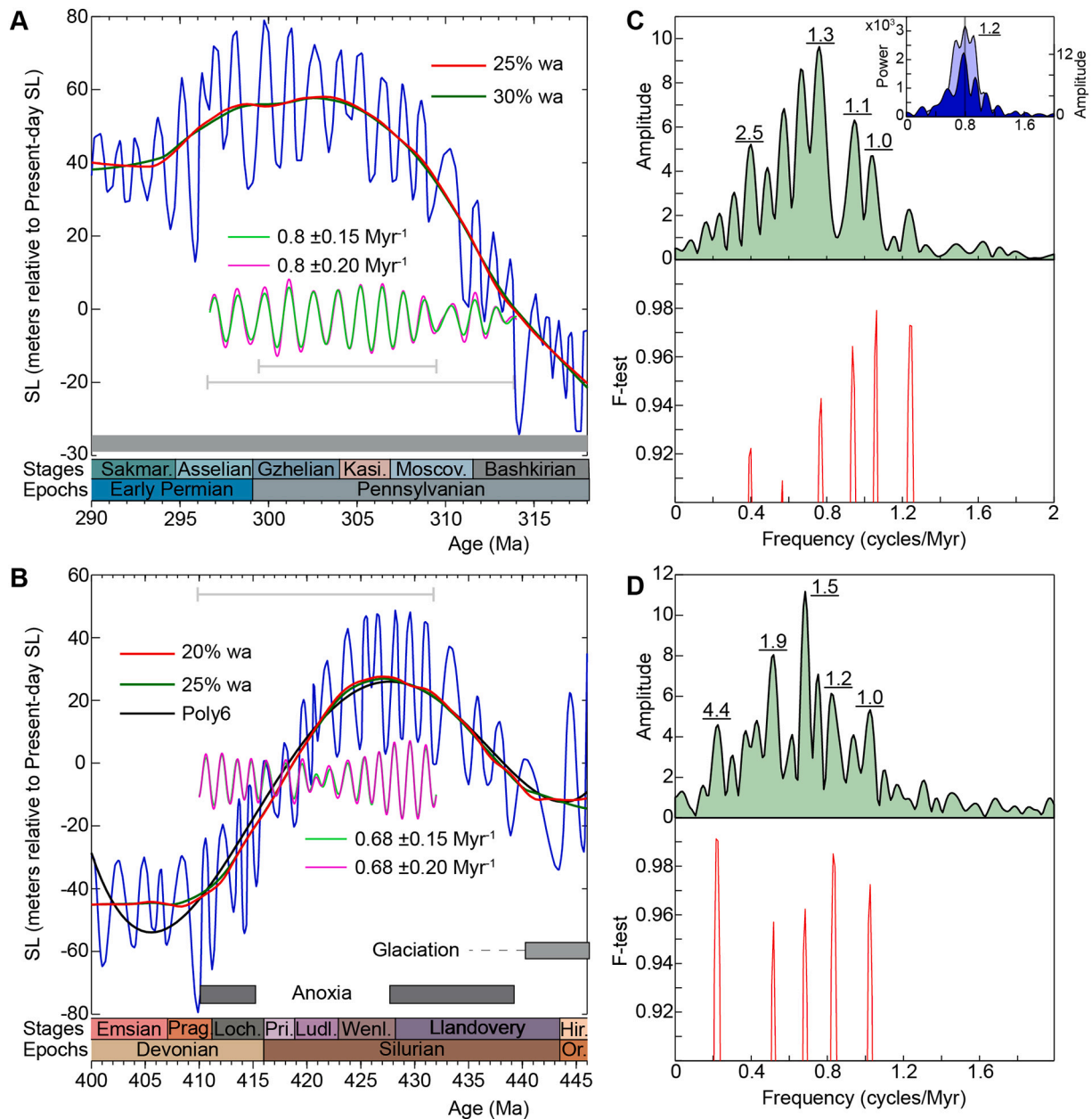


Fig. 15. Time-series analysis of some Paleozoic glaciated and partially glaciated intervals to highlight the 1 Myr scale sea-level cyclicality (third-order sequences, [Haq and Schutter, 2008](#)). (A) Pennsylvanian to Early Permian *p.p.* interval. Raw data (bleu) along with smoothing weighted average (wa), and bandpass filtering of two intervals (indicated by horizontal grey double-arrows) showing regular 1.2 Myr scale cyclicality (see spectra in 'C'). The grey horizontal bar indicates that all the interval is glaciated. (B) Silurian to Devonian *p.p.* interval. Raw data (bleu) along with smoothing weighted average (wa) and polynomial 6th order (Poly6), and bandpass filtering of one interval (indicated by horizontal grey double-arrow) showing regular 1.5 Myr scale cyclicality (see spectra in 'D'). The light-grey horizontal bar indicates the glaciated interval, and the dark-grey horizontal bar indicates the anoxic interval. (C) Spectrum of the interval from 296.7 to 314 Ma and the significance F-test (upper and lower panels, respectively). *Inset* in the upper panel: spectra of a short interval from 299.5 to 309.5 Ma showing a very regular cyclicality, depicted by a single strong peak centered on the period of 1.2 Myr. (D) Spectrum of the interval from 410 to 432 Ma and the significance F-test (upper and lower panels, respectively). All values of periods indicated on spectral peaks are labelled in Myr.

[Huybers and Curry, 2006](#); [Hinnov, 2013](#)). In other words, any change in the amplitude/frequency of the shorter cycles (seasonal/annual) would be transferred to the longer cycles (Milankovitch band and its modulations) in the volcanic record (e.g., [Mason et al., 2004](#); [Jupp et al., 2004](#); [Crowley et al., 2015](#); [Tolstoy, 2015](#)).

The above studies collectively suggest a potential connection between astro-climatically paced sea-level and Earth's interior and surface processes, depending on the presence or absence of icehouse conditions (i.e., via the annual hydrological cycle, [Mason et al., 2004](#)). Such connection may operate via a direct or indirect control of sea-level in

tune with seasonal/annual to Milankovitch scale variations. A direct control may be exerted by glacio-eustasy, aquifer-eustasy and/or thermo-eustasy (see Section 4.4). However, these mechanisms cannot explain the larger amplitudes of sea-level (hundred to several hundreds of meters), documented for the greenhouse periods. An indirect control may operate as feedbacks of Earth's interior to sea-level and Earth's surface perturbations from astronomical forcing. Earth's interior may resonate to these superficial perturbations in a similar fashion, as that suggested for the 100 kyr climate-glacial Quaternary cycles ([Crowley et al., 2015](#); [Tolstoy, 2015](#)).

Table 1

Hierarchy of sea-level sequences and their potential causal mechanisms (modified after Boulila et al., 2011, 2018, 2020). * Phanerozoic mean periodicity. Bold text indicates the updates. The ~35 Myr cyclicity has a very likely Milankovitch origin, which manifests as the modulator of the 10 Myr orbital band (present study). Precise secular frequencies of the 4.7 Myr orbital cycle are provided in Boulila (2019) and Boulila et al. (2020). The 9.5 Myr cycle originates from both the inclination and the eccentricity (Boulila, 2019) as well as the 4.7 Myr cycle (Boulila et al., 2012, 2020). Milankovitch forcing (eccentricity and inclination) by the 4.7, 9.5, 18 and 35 Myr orbital cycles induce perturbations in Earth's surface processes, transferred to the deep solid Earth, and the latter resonates in turn to such superficial perturbations, thus explaining the conjoint astronomical-tectonic forcing on sea-level change.

Order	Suborder	Mean period (Myr)	Causal mechanism	Astronomy
First	Longer	250–300*	Tectonic, galactic?	Radial motion?
	Shorter	91*	Tectonic, galactic?	
Second	Longer	36*	Milankovitch, tectonic	Eccentricity-Obliquity
	Medium-2	18	Milankovitch, tectonic	Eccentricity-Obliquity
	Medium-1	9.5*	Milankovitch, tectonic	Eccentricity-Obliquity
	Shorter	4.7	Milankovitch, tectonic?	Eccentricity-Obliquity
Third	Longer	2.4	Milankovitch	Eccentricity (g4-g3)
	Shorter	1.2	Milankovitch	Obliquity (s4-s3)
Fourth		0.405	Milankovitch	Eccentricity (g2-g5)
Fifth	Longer	0.173	Milankovitch	Obliquity
	Shorter	0.1	Milankovitch	Eccentricity
Sixth	Longer	0.04	Milankovitch	Obliquity
	Shorter	0.020	Milankovitch	Precession

Although we shed light on a continuum of astro-tectonically linked sea-level, from annual to 35 Myr cycle bands, with the available data it is hard to collectively envision the shorter, annual, and the longer, Myr to tens of Myr, timescales either in terms of sea-level magnitude or in terms of operating, forcing processes (e.g., Conrad, 2013). However, the Phanerozoic data allows the suggestion that magnitude of sea-level changes could be enhanced from higher to lower frequencies (energy-transfer process, Boulila et al., 2012), i.e., the longer climate-tectonic cycle the larger the sea-level magnitude is (Fig. 1). Therefore, low-frequency tectonic cycles and processes (Section 4.4), in response to climatically-driven mass changes on Earth's surface including rock accumulation and erosion (e.g., Calais et al., 2010; Sternai et al., 2016; Pesek et al., 2020), have the potential to explain larger sea-level magnitudes during greenhouse periods (e.g., Vail et al., 1977; Haq et al., 1987; Haq and Schutter, 2008; Müller et al., 2008; Conrad, 2013).

The 10 and 35 Myr cycles are common in Milankovitch, sea-level and subduction data. However, a dominant 25–26 Myr cyclicity has been detected in mid-ocean spreading data (Figs. 4 and 5, Cogné and Humler, 2006; Müller and Dutkiewicz, 2018). The 25–26 Myr cyclicity modulates the 10 Myr band in spreading and subduction data (Supplementary Information, Section 3.2). The present review points to a coupling between spreading and subduction at the 10 Myr band, but not at tens of Myr (Section 3.2). Such result should be further investigated in future geodynamic modeling efforts. Otherwise, one would expect that sea level oscillates in tune with mid-ocean spreading, given the potential link between them (e.g., Müller et al., 2008; see Conrad, 2013 for a review). However, subduction data also strongly correlate with sea level change (Figs. 13 and 14). We thus suggest that the long-term sea-level change is predominantly paced by the subduction processes. Recent studies of Earth's interior water cycling implies that the amount of water entering Earth's interior via subduction (Cai et al., 2018) greatly exceeds estimates of the amount being emitted by volcanoes including mid-ocean seafloor spreading (Parai and Mukhopadhyay, 2012), thus enhancing the importance of the subduction processes in the global water budget

(Shillington, 2018). Nevertheless, changes to sea-level from both the spreading and subduction processes, which respond in turn to long-term (tens of Myr) perturbations in Earth's surface systems, is likely (Section 4.4). Reciprocally, substantial release of carbon dioxide (CO₂) from mid-ocean ridges (Müller and Dutkiewicz, 2018) and from subduction zones (Van Der Meer et al., 2014) could equally influence climate change at tens of Myr time scales.

5. Conclusions

Superimposed on the tectono-eustatic Wilson megacycle (250–300 Myr in duration) are several long-term global sea level cyclicities of different amplitudes and origins. The most prominent ones are the ~10 and ~35 Myr cycles. Increasing evidence for Milankovitch orbital pacing of the ~10 Myr cyclicity has been demonstrated from various geological datasets and in the modulation of Milankovitch astronomical cycles. However, the origin of ~35 Myr eustatic cyclicity has been controversial, which has been ascribed either to tectonics or climate from the solar system motion in the Galaxy.

Here we have reviewed the origin of ~10 and ~35 Myr sea-level cycles based on amplitude modulation analysis of the compiled Phanerozoic sea-level data, together with additional geological datasets. We show that the 10 cycle band may be modulated by the ~35 Myr cyclicity in the sea-level record. We have tested the ~10 and ~35 Myr sea-level cyclicities for potential Milankovitch-forcing hypothesis since the 10 Myr cycle arises from amplitude modulation of Milankovitch cycle band. Amplitude modulation analysis of Earth's orbital eccentricity variations indicates the modulation of the ~10 Myr cycles by the ~35 Myr cyclicity in different astronomical models. A correlation between sea-level and astronomical (insolation) variations at these two cyclicities provides a compelling evidence for a link between the two.

Additionally, the sea-level data support theoretical modeling that predicts the validity of astronomical models as far back as 45 Ma. We also show that the La2004 astronomical model provides the best fit with sea-level record compared to the more recent La2010d model. In particular, a good correlation between sea-level and La2004 astronomical data was established up to 50 Ma at the 10 Myr cycle, and even almost up to 150 Ma for the 35 Myr cycle, pointing to the robustness of La2004 model.

Our review suggests that it is unnecessary to invoke astronomically paced 35 Myr cycle via cosmic ray flux from the vertical motion of solar system, unless insolation and cosmic ray are coupled through planetary and solar-system motions.

Finally, time-series analysis of subduction data from recent plate tectonic models also captures the 10 and 35 Myr cyclicities. These tectonic cyclicities, especially the 35 Myr cycle, correlated to sea-level and Milankovitch cycles. However, seafloor spreading data show a dominant cyclicity of 25–26 Myr. The interference of the 25–26 and 36 Myr (Phanerozoic mean period) tectonic cyclicities may explain a resulting third Phanerozoic sea-level cyclicity of a period that spans close to 91 Myr (1/26–1/35).

The record of similar cyclicities in sea-level, $\delta^{18}\text{O}$, Milankovitch and tectonic variations, and the correlations between them, especially at the 35 Myr band, suggest a coupling between Earth's surface and interior processes. We thus hypothesize that Earth's interior processes resonate with astro-climatically (Milankovitch) driven perturbations of Earth's surface that include sea-level fluctuations. Our review augments the broad conclusion is that sea-level changes can respond directly to Milankovitch orbital forcing via glacio-eustasy, thermo-eustasy and/or aquifer-eustasy or indirectly through feedbacks from tectonically-paced ocean-basin volume changes.

Declaration of Competing Interest

The authors declare that they have no known competing financial interests or personal relationships that could have appeared to influence

the work reported in this paper.

Acknowledgments

S.B., B.G. and G.C. were supported by the ANR *AstroMeso* and ERC *AstroGeo* projects. B.U.H. acknowledges the support of his Sorbonne tenure through a doctoral funding by Total, and his sabbatical at Utrecht University in 2019 by Royal Dutch Academy of Sciences. N.C.H. acknowledges the financial support of the National Centre for Competence in Research of the Swiss National Science Foundation (SNSF). RDM was supported by the AuScope National Collaborative Research Infrastructure System (NCRIS) program. We thank Steve Puetz and an anonymous reviewer for their very helpful constructive comments.

Appendix A. Supplementary data

Supplementary data to this article can be found online at <https://doi.org/10.1016/j.earscirev.2021.103727>.

References

- Abreu, V.S., Hardenbol, J., Haddad, G.A., Baum, G.R., Droxler, A.W., Vail, P.R., 1998. Oxygen isotope synthesis: A Cretaceous ice-house? In: de Graciansky, P.C., Jacquin, T., Hardenbol (Eds.), *Mezozoic and Cenozoic Sequence Stratigraphy of European Basins*. Vol. 60. SEPM Special Publication, Pp. 75–80. Soc Sediment Geol, Tulsa, OK.
- Austermann, J., Mitrovica, J.X., Latychev, K., Milne, G.A., 2013. Barbados-based estimate of ice volume at last Glacial Maximum affected by subducted plate. *Nat. Geosci.* 6, 553–557.
- Bacon, C.R., Lanphere, M.A., 2006. Eruptive history and geochronology of Mount Mazama and the Crater Lake region. *Oregon. Geol. Soc. Am. Bull.* 118, 1331–1359.
- Bailer-Jones, C.A.L., 2009. The evidence for and against astronomical impacts on climate change and mass extinctions: a review. *Int. J. Astrobiol.* 8, 213–239.
- Baker, R.G.V., Flood, P.G., 2015. The Sun-Earth connect 3: lessons from the periodicities of deep time influencing sea-level change and marine extinctions in the geological record. *SpringerPlus* 4, 285.
- Beaufort, L., 1994. Climatic importance of the modulation of the 100 kyr cycle inferred from 16 m.y. long Miocene records. *Paleoceanography* 9, 821–834.
- Berger, A., Loutre, M.F., Mélice, J.L., 2006. Equatorial insolation: from precession harmonics to eccentricity frequencies. *Clim. Past* 2, 131–136.
- Bond, D.P., Grasby, S.E., 2017. On the causes of mass extinctions. *Palaeogeogr. Palaeoclimatol. Palaeoecol.* 478, 3–29.
- Bornemann, A., Norris, R.D., Friedrich, O., Beckmann, B., Schouten, S., Damsté, J.S.S., Vogel, J., Hofmann, P., Wagner, T., 2008. Isotopic evidence for glaciation during the Cretaceous Supergreenhouse. *Science* 319, 189–192.
- Boulila, S., 2019. Coupling between Grand cycles and events in Earth's climate during the past 115 million years. *Sci. Rep.* 9, 327. <https://doi.org/10.1038/s41598-018-36509-7>.
- Boulila, S., Galbrun, B., Hinnov, L.A., Collin, P.Y., Ogg, J.G., Fortwengler, D., Marchand, D., 2010. Milankovitch and sub-Milankovitch forcing of the Oxfordian (late Jurassic) Terres Noires Formation (SE France) and global implications. *Basin Res.* 22, 717–732.
- Boulila, S., Galbrun, B., Miller, K.G., Pekar, S.F., Browning, J.V., Laskar, J., Wright, J.D., 2011. On the origin of Cenozoic and Mesozoic “third-order” eustatic sequences. *Earth-Sci. Rev.* 109, 94–112.
- Boulila, S., Galbrun, B., Laskar, J., Pälike, H., 2012. A ~9 myr cycle in Cenozoic $\delta^{13}C$ record and long-term orbital eccentricity modulation: is there a link? *Earth Planet. Sci. Lett.* 317–318, 273–281.
- Boulila, S., Galbrun, B., Huret, E., Hinnov, L.A., Rouget, I., Gardin, S., Bartolini, A., 2014. Astronomical calibration of the Toarcian Stage: implications for sequence stratigraphy and duration of the early Toarcian OAE. *Earth Planet. Sci. Lett.* 386, 98–111.
- Boulila, S., Laskar, J., Haq, B.U., Galbrun, B., Hara, N., 2018. Long-term cyclicities in Phanerozoic Sea-level sedimentary record and their potential drivers. *Global Planet. Change* 185, 129–136.
- Boulila, S., Brange, C., Cruz, A.M., Laskar, J., Gorini, C., Reis, T.D., Silva, C.G., 2020. Astronomical pacing of late Cretaceous third- and second-order sea-level sequences in the Foz do Amazonas Basin. *Mar. Pet. Geol.* 117, 104382.
- Braun, J., 2010. The many surface expressions of mantle dynamics. *Nat. Geosci.* 3 (12), 825–833.
- Cai, C., Wiens, D.A., Shen, W., Eimer, M., 2018. Water input into the Mariana subduction zone estimated from ocean-bottom seismic data. *Nature* 563, 389–392.
- Calais, E., Freed, A.M., Van Arsdale, R., Stein, S., 2010. Triggering of New Madrid seismicity by late-Pleistocene erosion. *Nature* 466, 608–611.
- Cerpa, N.G., Jones, D.W.R., Katz, R.F., 2019. Consequences of glacial cycles for magmatism and carbon transport at mid-ocean ridges. *Earth Planet. Sci. Lett.* 528, 115845.
- Čížková, H., Bina, C.R., 2015. Geodynamics of trench advance: Insights from a Philippine-Sea-style geometry. *Earth Planet. Sci. Lett.* 430, 408–415.
- Clark, J.A., Farrell, W.E., Peltier, W.R., 1978. Global changes in postglacial sea level: a numerical calculation. *Quat. Res.* 9 (3), 265–287.
- Cloetingh, S., Haq, B.U., 2015. Inherited landscapes and sea level change. *Science* 347, 393–403.
- Cogné, J.-P., Humler, E., 2006. Trends and rhythms in global seafloor generation rate. *Geochim. Geophys. Geosyst.* 7 <https://doi.org/10.1029/2005GC001148>. Q03011.
- Cogné, J.-P., Humler, E., 2008. Global scale patterns of continental fragmentation: Wilson's cycles as a constraint for long-term sea-level changes. *Earth Planet. Sci. Lett.* 273 (3–4), 251–259.
- Cogné, J.-P., Humler, E., Courtillot, V., 2006. Mean age of oceanic lithosphere drives eustatic sea-level change since Pangea breakup: Earth and Planetary Science Letters 245 (1–2), 115–122.
- Conrad, C.P., 2013. The solid Earth's influence on sea level. *GSA Bull.* 125 (7/8), 1027–1052.
- Conrad, C.P., 2015. How climate influences sea-floor topography. *Science* 347, 1204–1205.
- Conrad, C.P., Gurnis, M., 2003. Seismic tomography, surface uplift, and the breakup of Gondwanaland: Integrating mantle convection backwards in time. *Geochimistry Geophysics Geosystems* 4, 1031. <https://doi.org/10.1029/2001GC000299>.
- Conrad, C.P., Hager, B.H., 1997. Spatial variations in the rate of sea level rise caused by the present-day melting of glaciers and ice sheets. *Geophys. Res. Lett.* 24 (12), 1503–1506.
- Conrad, C.P., Lithgow-Bertelloni, C., Loudon, K.E., 2004. Iceland, the Farallon slab, and dynamic topography of the North Atlantic. *Geology* 32 (3), 177–180.
- Courtillot, V.E., Renne, P.R., 2003. On the ages of flood basalt events. *Compt. Rendus Geosci.* 335, 113–140.
- Crowley, J.W., Katz, R.F., Huybers, P., Langmuir, C.H., Park, S.-H., 2015. Glacial cycles drive variations in the production of oceanic crust. *Science* 347, 1237–1240.
- Damon, P.E., 1971. The relationship between late Cenozoic volcanism and tectonism and orogenic-peirogenic periodicity. In: Turekian, K.K. (Ed.), *The Late Cenozoic Glacial Ages*. New Haven. Yale University Press, Conn, pp. 15–35.
- Davies, A., Gréselle, B., Hunter, S.J., Baines, G., Robson, C., Haywood, A.M., Ray, D.C., Simmons, M.D., van Buchem, F.S.P., 2020. Assessing the impact of aquifer-eustasy on short-term Cretaceous. *Cret. Res.* 112, 104445.
- Davis, M., Hut, P., Muller, R.A., 1984. Extinction of species by periodic comet showers. *Nature* 308, 715–717.
- DeCelles, P.G., Ducea, M.N., Kapp, P., Zandt, G., 2009. Cyclicity in cordilleran orogenic systems. *Nat. Geosci.* 2, 251–257.
- Deynoux, M., Miller, J.M.G., Domack, E.W., Eyles, N., Fairchild, I.J., Young, G.M., 1994. *Earth's Glacial Record*. Cambridge University Press, Cambridge, p. 266.
- Dinger, F., Bredemeyer, S., Arellano, S., Bobrowski, N., Platt, U., Wagner, T., 2019. On the link between Earth tides and volcanic degassing. *Solid Earth* 10, 725–740.
- Dorman, F.H., 1968. Some Australian oxygen isotope temperatures and a theory for a 30-million-year world-temperature. *J. Geol.* 76, 297–313.
- Embry, S., Beauchamp, B., Dewing, K., Dixon, J., 2019. Episodic tectonics in the Phanerozoic succession of the Canadian high arctic and the “10-million-year flood”. In: Piepjohn, K., Strauss, J.V., Reinhardt, L., McClelland, W.C. (Eds.), *Circum-Arctic Structural Events: Tectonic Evolution of the Arctic Margins and Trans-arctic Links with Adjacent Orogens*, vol. 541. Geological Society of America Special Paper. [https://doi.org/10.1130/2018.2541\(11\)](https://doi.org/10.1130/2018.2541(11)).
- Emter, D., 1997. Tidal triggering of earthquakes and volcanic events. In: Bhattacharji, S., et al. (Eds.), *Tidal Phenomena*. Springer, New York, pp. 293–309.
- Fang, Q., Wu, H., Hinnov, L.A., Jing, X., Wang, X., Jiang, Q., 2015. Geologic evidence for chaotic behavior of the planets and its constraints on the third-order eustatic sequences at the end of the late Paleozoic Ice Age. *Palaeogeogr. Palaeoclimatol. Palaeoecol.* 440, 848–859.
- Farrell, W.E., 1972. Deformation of the Earth by surface loads. *Rev. Geophys. Space Phys.* 10 (3), 761–797.
- Farrell, W.E., Clark, J.A., 1976. On postglacial sea level. *Geophys. J. R. Astron. Soc.* 46 (3), 647–667.
- Fischer, A.G., 1984. Two Phanerozoic supercycles. In: Berggren, W.A., Van Couvering, J. A. (Eds.), *Catastrophes and Earth History*. Princeton University Press, Princeton, pp. 129–150.
- Fischer, A.G., Arthur, M.A., 1977. Secular variations in the pelagic realm. In: Cook, H.E., Enos, P. (Eds.), *Deep Water Carbonate Environments*, 25. Soc. Econ. Paleontol. Mineral. Spec. Publ., pp. 18–50.
- Flament, N., Gurnis, M., Müller, R.D., 2013. A review of observations and models of dynamic topography. *Lithosphere* 5, 189–210.
- Föllmi, K.B., 2012. Early Cretaceous life, climate and anoxia. *Cretac. Res.* 35, 230–257.
- Frakes, L.A., Francis, J.E., Syktus, J.L., 1992. *Climate Modes of the Phanerozoic: The History of the Earth's Climate over the Past 600 Million Years*. Cambridge University Press, Cambridge, p. 274.
- Gaffin, S., 1987. Ridge volume dependence on seafloor generation rate and inversion using long term sea level change. *Am. J. Sci.* 287 (6), 596–611.
- Galeotti, S., Rusciadelli, G., Sprovieri, M., Lanci, L., Gaudio, A., Pekar, S., 2009. Sea-level control on facies architecture in the Cenomanian–Coniacian Apulian margin (Western Tethys): a record of glacio-eustatic fluctuations during the Cretaceous greenhouse? *Palaeogeogr. Palaeoclimatol. Palaeoecol.* 276, 196–205.
- Ghil, M., Allen, R.M., Dettinger, M.D., Ide, K., Kondrashov, D., Mann, M.E., Robertson, A., Saunders, A., Tian, Y., Varadi, F., Yiou, P., 2002. Advanced spectral methods for climatic time series. *Rev. Geophys.* 40 (1), 3.1–3.41.
- Goff, J.A., Zahirovic, S., Müller, R.D., 2018. No evidence for Milankovitch cycle influence on abyssal hills at intermediate, fast, and superfast spreading rates. *Geophys. Res. Lett.* 45 (19), 10,305–10,313.
- Grabau, A.W., 1936. Oscillation or pulsation? International Geological Congress Report on the 16th session. USA 1933 (1), 539–552.

- Grabau, A.W., 1940. The Rhythm of the Ages. Henri Vetch Pub Peking China. 561p.
- Gradstein, F.M., Ogg, J.G., Schmitz, M.D., Ogg, G., 2020. Geological Time Scale 2020. Elsevier, Amsterdam.
- Gurnis, M., 1993. Phanerozoic marine inundation of continents driven by dynamic topography above subducting slabs. *Nature* 364 (6438), 589–593.
- Haq, B.U., 2018. Triassic eustatic variations re-examined. *GSA Today*, 28, 4–9 + Online supporting material, 16 pp. <https://doi.org/10.1130/GSATG381A.1>.
- Haq, B.U., Al-Qahtani, A.-M., 2005. Phanerozoic cycles of sea-level change on the Arabian platform. *GeoArabia* 10 (2), 127–160.
- Haq, B.U., Schutter, S.R., 2008. A chronology of Paleozoic Sea-level changes. *Science* 322 (5898), 64–68.
- Haq, B.U., Hardenbol, J., Vail, P.R., 1987. Chronology of fluctuating sea levels since the Triassic. *Science* 235 (4793), 1156–1167.
- Harrison, C.G.A., 1990. Long-term eustasy and epeirogeny in continents. In: Revelle, R.R. (Ed.), *Sea-Level Change: Washington*. National Academy Press, D.C., pp. 141–158.
- Haskell, N.A., 1935. The motion of a fluid under a surface load. *Physics Letters, Part B* 6, 265–269.
- Hinnov, L.A., 2000. New perspectives on orbitally forced stratigraphy. *Annu. Rev. Earth Planet. Sci.* 28, 419–475.
- Hinnov, L.A., 2013. Cyclostratigraphy and its revolutionizing applications in the earth and planetary sciences. *GSA Bull.* 125 (11/12), 1703–1734.
- Huang, C., Hinnov, L.A., Fischer, A.G., Grippo, A., Herbert, T., 2010. Astronomical tuning of the Aptian Stage from Italian reference sections. *Geology* 38, 899–902.
- Huybers, P., Curry, W., 2006. Links between annual, Milankovitch and continuum temperature variability. *Nature* 441, 329–332.
- Huybers, P., Denton, G., 2008. Antarctic temperature at orbital time scales controlled by local summer duration. *Nat. Geosci.* 1, 787–792.
- Huybers, P., Langmuir, C., 2009. Feedback between deglaciation, volcanism and atmospheric CO₂. *Earth Planet. Sci. Lett.* 286, 479–491.
- Huybers, P., Langmuir, C.H., 2017. Delayed CO₂ emissions from mid-ocean ridge volcanism as a possible cause of late-Pleistocene glacial cycles. *Earth Planet. Sci. Lett.* 457, 238–249.
- Immenhauser, A., 2005. High-rate Sea-level change during the Mesozoic: New approaches to an old problem. *Sediment. Geol.* 175, 277–296.
- Jacobs, D.K., Sahagian, D.L., 1993. Climate-induced fluctuations in sea level during non-glacial times. *Nature* 361, 710–712.
- Jacobs, D.K., Sahagian, D.L., 1995. Milankovitch Fluctuations in Sea Level and recent Trends in Sea-Level Change: Ice may not always be the answer. In: Haq, B.U. (Ed.), *Sequence Stratigraphy and Depositional Response to Eustatic, Tectonic and Climatic Forcing*. Springer Netherlands, Dordrecht, pp. 329–366.
- Jellinek, A.M., Manga, M., Saar, M.O., 2004. Did melting glaciers cause volcanic eruptions in eastern California? Probing the mechanics of dike formation. *J. Geophys. Res., Solid Earth* (1978–2012) 109.
- John, C.M., Karner, G.D., Mutti, M., 2004. $\delta^{18}\text{O}$ and Marion Plateau backstripping: Combining two approaches to constrain latemiddle Miocene eustatic amplitude. *Geology* 32, 829–832.
- Johnston, M., Mauk, F., 1972. Earth Tides and the triggering of Eruptions from Mt Stromboli, Italy. *Nature* 239, 266–267.
- Jupp, T.E., Pyle, D.M., Mason, B.G., Dade, W.B., 2004. A statistical model for the timing of earthquakes and volcanic eruptions influenced by periodic processes. *J. Geophys. Res.* 109 <https://doi.org/10.1029/2003JB002584>. B02206.
- Kaiho, K., Saito, S., 1994. Oceanic crust production and climate during the last 100 Ma. *Terra Nova* 6, 376–384.
- Karlsen, K.S., Conrad, C.P., Magni, V., 2019. Deep water cycling and sea level change since the breakup of Pangea. *Geochim. Geophys. Geosyst.* 20 (6), 2919–2935.
- Kitchell, J.A., Pena, D., 1984. Periodicity of extinctions in the geologic past: deterministic versus stochastic explanations. *Science* 226 (4675), 689–692.
- Kominz, M.A., Browning, J.V., Miller, K.G., Sugarman, P.J., Mizintseva, S., Scotese, C.R., 2008. Late cretaceous to Miocene Sea-level estimates from the New Jersey and Delaware coastal plain coreholes: an error analysis. *Basin Res.* 20, 211–226.
- Kutterolf, S., Jegen, M., Mitrovica, J.X., Kwasnitschka, T., Freundt, A., Huybers, P., 2012. A detection of Milankovitch frequencies in global volcanic activity. *Geology* 41, 227–230.
- Lagabriele, Y., Goddérès, Y., Donnadié, Y., Malavieille, J., Suarez, M., 2009. The tectonic history of Drake Passage and its possible impacts on global climate. *Earth Planet. Sci. Lett.* 279, 197–211.
- Lamb, S., Davis, P., 2003. Cenozoic climate change as a possible cause for the rise of the Andes. *Nature* 425, 792–797.
- Laskar, J., 1990. The chaotic motion of the Solar System: a numerical estimate of the size of the chaotic zone. *Icarus* 88, 266–291.
- Laskar, J., 1999. The limits of the Earth orbital calculations for geological time-scale use. *Philos. Trans. R. Soc. Lond. A* 357, 1735–1759.
- Laskar, J., Joutel, F., Boudin, F., 1993. Orbital, precessional, and insolation quantities for the Earth from –20 Myr to +10 Myr. *Astron. Astrophys.* 270, 522–533.
- Laskar, J., Robutel, P., Joutel, F., Gastineau, M., Correia, A.C.M., Levrard, B., 2004. A long-term numerical solution for the insolation quantities of the Earth. *Astron. Astrophys.* 428, 261–285.
- Laskar, J., Fienga, A., Gastineau, M., Manche, H., 2011. La2010: a new orbital solution for the long term motion of the Earth. *Astronomy and Astrophysics* 532. <https://doi.org/10.1051/0004-6361/201116836>. A89.
- Li, M., Hinnov, L.A., Huang, C., Ogg, J.G., 2018. Sedimentary noise and sea levels linked to land–ocean water exchange and obliquity forcing. *Nat. Commun.* 9, 1004.
- Li, M., Hinnov, L., Kump, L., 2019. Acycle: Time-series analysis software for paleoclimate projects and education. *Comput. Geosci.* 127, 12–22.
- Lieberman, B.S., Melott, A.L., 2007. Considering the Case for Biodiversity Cycles: Reexamining the evidence for Periodicity in the Fossil Record. *PLoS One* 2 (8). <https://doi.org/10.1371/journal.pone.0000759>. e759.
- Liu, Y., Huang, C., Ogg, J.G., Algeo, T.J., Kemp, D.B., Shen, W., 2019. Oscillations of global sea-level elevation during the Paleogene correspond to 1.2-Myr amplitude modulation of orbital obliquity cycles. *Planet. Sci. Lett.* 522, 65–78.
- Lombard, A., Cazenave, A., Le Traon, P.-Y., Ishii, M., 2005. Contribution of thermal expansion to present day sea-level change revisited. *Glob. Planet. Chang.* 47 (1), 1–16.
- Lovell, B., 2010. A pulse in the planet: Regional control of high-frequency changes in relative sea level by mantle convection. *J. Geol. Soc. Lond.* 167 (4), 637–648.
- Lund, D.C., Asimow, P.D., 2011. Does sea level influence mid-ocean ridge magmatism on Milankovitch timescales? *Geochim. Geophys. Geosyst.* 12.
- MacLennan, J., Jull, M., McKenzie, D., Slater, L., Grönvold, K., 2002. The link between volcanism and deglaciation in Iceland. *Geochim. Geophys. Geosyst.* 3, 1–25.
- Mason, B.G., Pyle, D.M., Dade, W.B., Jupp, T., 2004. Seasonality of volcanic eruptions. *J. Geophys. Res.* 109 <https://doi.org/10.1029/2002JB002293>. B04206.
- Matthews, R.K., 1984. Oxygen-isotopic record of ice-volume history: 100 million years of glacioeustatic fluctuations. *AAPG Mem.* 36, 97–107.
- Matthews, R.K., Al-Husseini, M.I., 2010. Orbital-forcing glacio-eustasy: a sequence stratigraphic time scale. *GeoArabia* 15, 129–142.
- McGuire, W.J., Howarth, R.J., Firth, C.R., Solow, A.R., Pullen, A.D., Saunders, S.J., Stewart, I.S., Vita-Finzi, C., 1997. Correlation between rate of sea-level change and eny of explosive volcanism in the Mediterranean. *Nature* 389, 473–476.
- McNutt, S.R., Beavan, R.J., 1981. Volcanic earthquakes at Pavlov Volcano correlated with the solid earth tide. *Nature* 294, 615–618.
- McNutt, S.R., Beavan, R.J., 1980. Patterns of earthquakes and the effect of solid earth and ocean load tides at Mount St. Helens prior to the May 18, 1980, eruption. *J. Geophys. Res.-Sol. Ea.* 89, 3075–3086.
- Medvedev, M.V., Melott, A.L., 2007. Do extragalactic cosmic rays induce cycles in fossil diversity? *Astrophys. J.* 664, 879–889.
- Melott, A.L., Bambach, R.K., 2010. Nemesis reconsidered. *Monthly Notices of the Royal Astronomical Society Letters* 407, L99–L102.
- Melott, A.L., Bambach, R.K., 2014. Analysis of periodicity of extinction using the 2012 geological time scale. *Paleobiology* 40, 177–196.
- Métivier, L., Greff-Lefftz, M., Altamimi, Z., 2010. On secular geocenter motion: the impact of climate changes. *Earth Planet. Sci. Lett.* 296 (3–4), 360–366.
- Miller, K.G., Sugarman, P.J., Browning, J.V., Kominz, M.A., Hernandez, J.C., Olsson, R. K., Wright, J.D., Feigenson, M.D., Van Sickle, W., 2003. A chronology of late cretaceous sequences and sea-level history: glacioeustasy during the Greenhouse World. *Geology* 31, 585–588.
- Miller, K.G., Sugarman, P.J., Browning, J.V., Kominz, M.A., Olsson, R.K., Feigenson, M. D., Hernandez, J.C., 2004. Upper cretaceous sequences and sea-level history, New Jersey Coastal Plain. *Geol. Soc. Am. Bull.* 116, 368–393.
- Miller, K.G., Kominz, M.A., Browning, J.V., Wright, J.D., Mountain, G.S., Katz, M.E., Sugarman, P.J., Cramer, B.S., Christie-Blick, N., Pekar, S.F., 2005a. The Phanerozoic record of global sea-level change. *Science* 310, 1293–1298.
- Miller, K.G., Wright, J.D., Browning, J.V., 2005b. Visions of ice sheets in a greenhouse world. *Mar. Geol.* 217, 215–231.
- Miller, et al., 2020. Cenozoic sea-level and cryospheric evolution from deep-sea geochemical and continental margin records. *Sci. Adv.* 6 eaaz1346.
- Mitchell, R.N., Bice, D.M., Montanari, A., Cleavel, L.C., Christianson, K.T., Coccioni, R., Hinnov, L.A., 2008. Oceanic Anoxic Cycles? Orbital prelude to the Bonarelli Level (OAE 2). *Earth Planet. Sci. Lett.* 267, 1–16.
- Mitchell, R.N., Spencer, C.J., Kirschner, U., He, X.-F., Murphy, J.B., Li, Z.-X., Collins, W.J., 2019. Harmonic hierarchy of mantle and lithospheric convective cycles: Time series analysis of hafnium isotopes of zircon. *Gondwana Res.* 75, 239–248.
- Mitrovica, J.X., Milne, G.A., 2002. On the origin of late Holocene Sea-level highstands within equatorial ocean basins. *Quat. Sci. Rev.* 21 (20–22), 2179–2190.
- Mitrovica, J.X., Peltier, W.R., 1991. On postglacial geoid subsidence over the equatorial oceans. *Journal of Geophysical Research-Solid Earth* 96, 20,053–20,071.
- Mitrovica, J.X., Peltier, W.R., 1993. Present-day secular variations in the zonal harmonics of Earth's geopotential. *Journal of Geophysical Research-Solid Earth* 98, 4509–4526.
- Mjelde, R., Wessel, P., Müller, R.D., 2010. Global pulsations of intraplate magmatism through the Cenozoic. *Lithosphere* 2, 361–376.
- Molnar, P., England, P., 1990. Late Cenozoic uplift of mountain ranges and global climate change: chicken or egg? *Nature* 346, 29–34.
- Moucha, R., Forte, A.M., Mitrovica, J.X., Rowley, D.B., Quere, S., Simmons, N.A., Grand, S.P., 2008. Dynamic topography and long-term sea-level variations: there is no such thing as a stable continental platform. *Earth Planet. Sci. Lett.* 271 (1–4), 101–108.
- Müller, R.D., Dutkiewicz, A., 2018. Ocean crustal carbon cycle drives 26-million years atmospheric carbon dioxide periodicities. *Science Advances* 4 (2) eaq0500.
- Müller, R.D., Scrolias, M., Gaina, C., Steinberger, B., Heine, C., 2008. Long-term sea-level fluctuations driven by ocean basin dynamics. *Science* 319, 1357–1362.
- Müller, R.D., Seton, M., Zahirovic, S., Williams, S.E., Matthews, K.J., Wright, N.M., Shephard, G.E., Maloney, K.T., Barnett-Moore, N., Hosseinpour, M., Bower, D.J., Cannon, J., 2016. Ocean basin evolution and global-scale plate reorganization events since Pangea breakup. *Annu. Rev. Earth Planet. Sci.* 44, 107–138.
- Müller, R.D., Hassan, R., Gurnis, M., Flament, N., Williams, S.E., 2018. Dynamic topography of passive continental margins and their hinterlands since the cretaceous. *Gondwana Res.* 53, 225–251.
- Müller, R.D., et al., 2019. A Global Plate Model Including Lithospheric Deformation along Major Rifts and Orogens since the Triassic. *Tectonics* 38, 1884–1907.

- Nakada, M., Lambeck, K., 1989. Late Pleistocene and Holocene Sea-level change in the Australian region and mantle rheology. *Geophys. J. Int.* 96, 497–517.
- Napier, W.N., 1988. NEOs and impacts: the Galactic connection. *Celest. Mech. Dyn. Astron.* 69, 59–75.
- Nerem, R.S., Wahr, J., 2011. Recent changes in the Earth's oblateness driven by Greenland and Antarctic ice mass loss. *Geophys. Res. Lett.* 38 (13) <https://doi.org/10.1029/2011GL047879>. L13501.
- Neuberg, J., 2000. External modulation of volcanic activity. *Geophys. J. Int.* 142, 232–240.
- Nowell, D., Jones, C., Pyle, D., 2006. Episodic Quaternary volcanism in France and Germany. *J. Quatern. Sci.* 21, 645–675.
- Olive, J.A., Behn, M.D., Ito, G., Buck, W.R., Escartín, J., Howell, S., 2015. Sensitivity of seafloor bathymetry to climate-driven fluctuations in mid-ocean ridge magma supply. *Science* 350 (6258), 310–313.
- Paillard, D., Labeyrie, L., Yiou, P., 1996. Macintosh program performs timeseries analysis. *Eos* 77, 379.
- Pälike, H., Norris, R.D., Herrle, J.O., Wilson, P.A., Coxall, H.K., Lear, C.H., Shackleton, N. J., Tripati, A.K., Wade, B.S., 2006. The Heartbeat of the Oligocene climate System. *Science* 314, 1894–1898.
- Parai, R., Mukhopadhyay, S., 2012. How large is the subducted water flux? New constraints on mantle regassing rates. *Earth Planet. Sci. Lett.* 317–318, 396–406.
- Peltier, W.R., Fairbanks, R.G., 2006. Global glacial ice volume and last Glacial Maximum duration from an extended Barbados Sea level record. *Quat. Sci. Rev.* 25, 3322–3337.
- Pesek, M.E., Perez, N.D., Meigs, A., Rowden, C.C., Giles, S., 2020. Exhumation timing in the Oregon Cascade Range decoupled from deformation, magmatic, and climate patterns. *Tectonics* 39. <https://doi.org/10.1029/2020TC006078>. e2020TC006078.
- Petersen, K.D., Nielsen, S.B., Clausen, O.R., Stephenson, R., Gerya, T., 2010. Small scale mantle convection produces stratigraphic sequences in sedimentary basins. *Science* 329 (5993), 827–830.
- Petrosino, S., Cusano, P., Madonia, P., 2018. Tidal and hydrological periodicities of seismicity reveal new risk scenarios at Campi Flegrei caldera. *Sci. Rep.* 8, 13808.
- Pitman, W.C., 1978. Relationship between eustasy and stratigraphic sequences of passive margins. *Geol. Soc. Am. Bull.* 89 (9), 1389–1403.
- Puetz, S.J., Borchardt, G., 2015. Quasi-periodic fractal patterns in geomagnetic reversals, geological activity, and astronomical events. *Chaos Solitons and Fractals* 81, 246–270.
- Puetz, S.J., Ganade, C.E., Zimmermann, U., Borchardt, G., 2018. Statistical analyses of Global U-Pb Database 2017. *Geosci. Front.* 9, 121–145.
- Rampino, R.M., 2010. Mass extinctions of life and catastrophic flood basalt volcanism. *Proc. Nat. Acad. Sci. USA* 107 (15), 6555–6556.
- Rampino, M.R., 2015. Dark matter in the Galaxy and potential cycles of extraterrestrial impacts, mass extinctions and geological events. *Mon. Not. R. Astron. Soc.* 448, 1816–1819.
- Rampino, M.R., Caldeira, K., 1993. Major episodes of geologic change: correlations, time structure and possible causes. *Earth Planet. Sci. Lett.* 114, 215–227.
- Rampino, M.R., Caldeira, K., 2015. Periodic impact cratering and extinction events over the last 260 million years. *Mon. Not. R. Astron. Soc.* 454, 3480–3484.
- Rampino, M.R., Caldeira, K., 2020. A 32-million year cycle detected in sea-level fluctuations over the last 545 Myr. *Geoscience Frontiers* 1029. <https://doi.org/10.1016/j.gsf.2020.06.005>.
- Rampino, M.R., Stothers, R.B., 1984. Geological rhythms and cometary impacts. *Science* 226, 1427–1431.
- Rampino, M.R., Stothers, R.B., 1988. Flood basalt volcanism during the past 250 million years. *Science* 241, 663–668.
- Rampino, M.R., Self, S., Fairbridge, R.W., 1979. Can rapid climatic change cause volcanic eruptions? *Science* 206, 826–829.
- Randal, L., Reece, M., 2014. Dark matter as a trigger for periodic comet impacts. *Phys. Rev. Lett.* 112, 161301.1–161301.5.
- Rasmussen, C.E., Williams, C.K.I., 2006. *Gaussian Processes for Machine Learning*. ISBN-13 978-0-262-18253-9.
- Raup, D.M., Sepkoski, J.J., 1984. Periodicity of extinctions in the geologic past. *Proc. Natl. Acad. Sci. U. S. A.* 81, 801–805.
- Raup, D.M., Sepkoski, J.J., 1988. Testing for periodicity of extinction. *Science* 241, 94–96.
- Ray, D.C., van Buchem, F.S.P., Baines, G., Davies, A., Gréselle, B., Simmons, M.D., Robson, C., 2019. The magnitude and cause of short-term eustatic cretaceous sea-level change: a synthesis. *Earth Sci. Rev.* 197, 102901.
- Raymo, M., Ruddiman, W.F., 1992. Tectonic forcing of late Cenozoic climate. *Nature* 359, 117–122.
- Raymo, M., Ruddiman, W.F., Froelich, P.N., 1988. Influence of late Cenozoic mountain building on ocean geochemical cycles. *Geology* 16 (7), 649–653.
- Rich, J.E., Johnson, G.L., Jones, J.E., Campsie, J., 1986. A significant correlation between fluctuations in seafloor spreading rates and evolutionary pulsations. *Paleoceanography* 1, 85–95.
- Rietbroek, R., Brunnabend, S.E., Kusche, J., Schröter, J., 2012. Resolving Sea level contributions by identifying fingerprints in time-variable gravity and altimetry. *J. Geodyn.* 59–60, 72–81.
- Roy, K., Peltier, W.R., 2011. GRACE era secular trends in Earth rotation parameters: a global scale impact of the global warming process? *Geophys. Res. Lett.* 38 (10) <https://doi.org/10.1029/2011GL047282>. L10306.
- Royer, D.L., Berner, R.A., Montañez, I.P., Tabor, N.J., Beerling, D.J., 2004. CO₂ as a primary driver of Phanerozoic climate. *GSA Today* 14, 4–10.
- Sames, B., Wagreich, M., Wendler, J.E., Haq, B.U., Conrad, C.P., Melinte-Dobrinescu, M. C., Hu, X., Wendler, I., Wolfgring, E., Yilmaz, I., Zorina, S.O., 2016. Review: Short Term Sea-Level Changes in a Greenhouse World — A View from the Cretaceous.
- Sames, B., Wagreich, M., Conrad, C.P., Iqbal, S., 2020. Aquifer-eustasy as the main driver of short-term sea-level fluctuations during Cretaceous hothouse climate phases. *Geological Society London Special Publications* 498. <https://doi.org/10.1144/SP498-2019-105>.
- Schindlbeck, J.C., Jegen, M., Freundt, A., Kutterolf, S., Straub, S.M., Mleneck-Vautravers, M.J., McManus, J., 2018. 100-kyr cyclicity in volcanic ash emplacement: evidence from a 1.1 Myr tephra record from the NW Pacific. *Scientific Reports*. <https://doi.org/10.1038/s41598-018-22595-0>.
- Shackleton, N.J., Imbrie, J., 1990. The $\delta^{18}\text{O}$ spectrum of oceanic deepwater over a 5-decade band. *Clim. Chang.* 16, 217–230.
- Shillington, 2018. Water takes a deep dive into the Mariana Trench. *Nature* 563, 335–336.
- Siddall, M., Hönisch, B., Waelbroeck, C., Huybers, P., 2010. Changes in deep Pacific temperature during the mid-Pleistocene transition and Quaternary. *Quat. Sci. Rev.* 29, 170–181.
- Simmons, M.D., 2012. Sequence stratigraphy and sea-level change. In: Gradstein, F.M., Ogg, J.G., Schmitz, M.D., Ogg, G.M. (Eds.), *The Geologic Time Scale 2012*, vol. 1, pp. 239–267.
- Simmons, M.D., Miller, K.G., Ray, D.C., Davies, A., van Buchem, F.S.P., Gréselle, B., 2020. Phanerozoic eustasy. In: Gradstein, F.M., Ogg, J.G., Schmitz, M.D., Ogg, G.M. (Eds.), *The Geologic Time Scale 2020* (in press). v.x, pp. xxx–xxx.
- Spasojevic, S., Gurnis, M., 2012. Sea level and vertical motion of continents from dynamic Earth models since the Late Cretaceous. *American Association of Petroleum Geologists Bulletin* 96 (11), 2037–2064.
- Sprovieri, M., Sabatino, N., Pelosi, N., Batenburg, S.J., Cocconeri, R., Iavarone, M., Mazzola, S., 2013. Late cretaceous orbitally-paced carbon isotope stratigraphy from the Bottaccione Gorge (Italy). *Palaeogeogr. Palaeoclimatol. Palaeoecol.* 379–380, 81–94.
- Sternai, P., Caricchi, L., Castelltort, S., Champagnac, J.-D., 2016. Deglaciation and glacial erosion: a joint control on magma productivity by continental unloading. *Geophys. Res. Lett.* 43, 1632–1641.
- Sternai, P., Caricchi, L., Pasquero, C., Garzanti, E., van Hinsbergen, D.J.J., Castelltort, S., 2020. Magmatic forcing of Cenozoic climate? *Journal of Geophysical Research: Solid Earth* 125. <https://doi.org/10.1029/2018JB016460>. e2018JB016460.
- Stigler, S.M., Wagner, M.J., 1987. A substantial bias in nonparametric tests for periodicity in geophysical data. *Science* 238, 940–945.
- Stigler, S.M., Wagner, M.J., 1988. Testing for periodicity of extinction: response. *Science* 241, 96–99.
- Stoll, H.M., Schrag, D.P., 1996. Evidence for glacial control of rapid sea level changes in the early cretaceous. *Science* 272, 1771–1774.
- Stoll, H.M., Schrag, D.P., 2000. High-resolution stable isotope records from the Upper cretaceous rocks of Italy and Spain: glacial episodes in a greenhouse planet? *Geol. Soc. Am. Bull.* 112, 308–319.
- Stothers, R.B., 1998. Galactic disk dark matter, terrestrial impact cratering and the law of large numbers. *Mon. Not. R. Astron. Soc.* 300, 1098–1104.
- Strasser, A., Hilgen, F.J., Heckel, P.H., 2006. Cyclostratigraphy – concepts, definitions, and applications. *News. Stratigr.* 42 (2), 75–114.
- Svensmark, H., 2006. Imprint of Galactic dynamics on Earth's climate. *Astron. Nachr. AN* 327 (9), 866–870.
- Svensmark, H., 2007. Cosmoclimatology: a new theory emerges. *Astron. Geophys.* 48, 1.18–1.24.
- Thomson, D.J., 1982. Spectrum estimation and harmonic analysis. *IEEE Proc.* 70, 1055–1096.
- Tolstoy, M., 2015. Mid-ocean ridge eruptions as a climate valve. *Geophys. Res. Lett.* 42, 1346–1351.
- Vail, P.R., Mitchum, R.M., Thompson, S., 1977. Seismic stratigraphy and global changes of sea level: Part 4. Global cycles of relative changes of sea level. In: Payton, C.E. (Ed.), *Seismic Stratigraphy, Applications to Hydrocarbon Exploration*. American Association of Petroleum Geologists Memoir, vol. 26, pp. 83–97.
- Van Der Meer, D.G., Zeebe, R.E., van Hinsbergen, D.J.J., Sluijs, A., Spakman, W., Torsvik, T.H., 2014. Plate tectonic controls on atmospheric CO₂ levels since the Triassic. *PNAS* 111 (22), 4380–4385.
- Wagreich, M., Lein, R., Sames, B., 2014. Eustasy, its controlling factors, and the limno-eustatic hypothesis e concepts inspired by Eduard Suess. *Austrian Journal of Earth Sciences* 107 (1), 115–131.
- Walcott, R.I., 1972. Past sea levels, eustasy and deformation of the Earth. *Quat. Res.* 2 (1), 1–14.
- Wendler, J.E., Wendler, I., 2016. What drove sea-level fluctuations during the mid-cretaceous greenhouse climate? *Palaeogeogr. Palaeoclimatol. Palaeoecol.* 441, 412–419.
- Wendler, J.E., Wendler, I., Vogt, C., Kuss, J., 2016. Link between cyclic eustatic sea-level change and continental weathering: evidence for aquifer-eustasy in the cretaceous. *Palaeogeogr. Palaeoclimatol. Palaeoecol.* 441 (3), 430–437.
- Whipple, K.X., 2009. The influence of climate on the tectonic evolution of mountain belts. *Nature Geosciences* 2, 97–104.
- Whiteside, J.H., Olsen, P.E., Eglinton, T., Brookfield, M.E., Sambrotto, R.N., 2010. Compound-specific carbon isotopes from Earth's largest flood basalt province directly link eruptions to the end-Triassic mass extinction. *Proc. Natl. Acad. Sci. U. S. A.* 107 (15), 6721–6725.
- Wiemer, D., Schrank, C.E., Murphy, D.T., Wenham, L., Allen, C.M., 2018. Earth's oldest stable crust in the Pilbara Craton formed by cyclic gravitational overturns. *Nat. Geosci.* 11, 357–361.
- Wise, D.U., 1974. In: Burh, C.A., Drake, C.L. (Eds.), *Continental Margins Freeboard and the Volumes of Continents and Oceans through Time. Geology of the continental margins* Springer Verlag Heidelberg Germany, pp. 45–58.

- Wolfram, L.C., Weinberg, R.F., Nebel, O., Hamza, K., Hasalová, P., Míková, J., Becchio, R., 2019. A 60-Myr record of continental back-arc differentiation through cyclic melting. *Nat. Geosci.* 12, 215–219.
- Wright, N.M., Seton, M., Williams, S.E., Whittaker, J.M., Müller, R.D., 2020. Sea level fluctuations driven by changes in global ocean basin volume following supercontinent break-up. *Earth Sci. Rev.* 208, 103293.
- Zachos, J.C., Pagani, M., Sloan, L., Thomas, E., Billups, K., 2001. Trends, rhythms, aberrations in global climate 65 Ma to present. *Science* 292, 686–693.
- Zucker, S., 2018. Detection of periodicity based on independence tests - III. Phase distance correlation periodogram. *Mon. Not. R. Astron. Soc. Lett.* 474 (1), L86–L90.